A NEW PARADIGM FOR KNOWLEDGE DISCOVERY AND DESIGN IN NANOPHOTONICS BASED ON ARTIFICIAL INTELLIGENCE

A Dissertation
Presented to
The Academic Faculty

by

Yashar Kiarashinejad

In Partial Fulfillment
of the Requirements for the Degree
Doctor of Philosophy in the
School of Electrical and Computer Engineering

Georgia Institute of Technology
December 2021

A NEW PARADIGM FOR KNOWLEDGE DISCOVERY AND DESIGN IN NAOPHOTONICS BASED ON ARTIFICIAL INTELLIGENCE

Approved by:

Professor Ali Adibi, Advisor
School of Electrical and Computer Engineering
Georgia Institute of Technology

Professor Hua Wang
School of Electrical and Computer Engineering
Georgia Institute of Technology

Professor Stephen E. Ralph
School of Electrical and Computer Engineering
Georgia Institute of Technology

Professor Benjamin Klein
School of Electrical and Computer Engineering
Kennesaw State University

Professor Haomin Zhou
School of Mathematics
Georgia Institute of Technology

Date Approved: August 3rd, 2021

ACKNOWLEDGEMENTS

TABLE OF CONTENTS

LIST OF TABLES

LIST OF FIGURES

SUMMARY

The design of photonic devices in the nanoscale regime for outperforming the bulky optical components has been a long-lasting challenge in state-of-the-art applications. Accordingly, devising a comprehensive model to understand and explain the physics and dynamics of light-matter interaction in these nanostructures is a substantial step toward discovering novel phenomena and nanophotonic devices. However, the systematic realization of mature optical functionalities using complex nanostructures requires significant knowledge about the influence of different nanostructure features (or design parameters) on the interaction with electromagnetic (EM) waves. Currently, this information can only be found using cumbersome numerical simulations, which become intractable as the number of design parameters increase. Despite extensive efforts in forming new approaches for analysis, design, and optimization of photonic nanostructures using semi-analytical modeling, computationally efficient methods for either understanding the physics of light-matter interaction in these nanostructures or their inverse design for achieving the desired response are still missing. This challenge is constantly worsened as the advances in nanofabrication technology provide more degrees of freedom (and a more significant number of design parameters) in forming functional photonic nanostructures.

In this thesis, I present a series of analysis and design approaches based on utilizing the "intelligent" aspects of artificial intelligence (AI). Applying these methods is beyond just designing the complex photonic nanostructures; they provide a powerful tool for a detailed understanding of the physics of light-matter interaction and discovering new

phenomena that can offer new classes of nanophotonic devices. Due to having a large number of design parameters and the complex and non-unique nature of the input-output relations in nanophotonic structures, conventional approaches cannot be used for their design and analysis. The dimensionality reduction (DR) techniques in this research considerably reduce the computing requirements. At the same time, machine-learning approaches like manifold learning and convex-hull formation enable the systematic evolution from an initial design to an optimal one.

Towards designing nanophotonic structures, I have developed a series of algorithms for knowledge discovery in nanophotonics. I have invented the shallow pseudo-encoder architecture to study the importance of each design parameter in forming the optical response. In follow-up research, I have introduced geometric learning approaches for studying the feasibility of the desired response using a class of photonic nanostructure while having a set of material and geometric constraints (e.g., the shape of nano cells or the optical properties of the available materials). In the final part of the trio, I have developed a new toolkit based on manifold learning to extract the underlying behaviors of responses for different classes of photonic nanostructures. Also, I have shown that we could extensively reduce the complexity of the neural network (NN) models by using pruning techniques. That would be a blessing for knowledge discovery in nanophotonics as one could dig into the deeper layers of the NN with reasonable complexity.

This thesis also focuses on developing a reliable inverse design approach by overcoming the non-uniqueness challenge. I have developed a double-step DR technique to reduce the complexity of the inverse design problem while preserving the necessary information for finding the optimum nanostructure for the desired functionality. I have

established an approach based on defining physics-driven metrics to explore the low-dimensional manifold of the design-response space and provide an optimal region in the reduced design space for the desired functionality. Also, I have employed probabilistic models to map the low-dimensional instances to the actual design parameters to complete the inverse design approach for non-unique problems.

Although the AI approaches developed in this thesis are used for knowledge discovery and inverse design of nanophotonic structures, they can be adopted and extended to a wide range of engineering and science disciplines where the computational requirements of the conventional design and analysis techniques make them impossible to use for design and knowledge discovery. As an example, the manifold-learning approach was recently extended to the classification of the severity of COVID-19 and the discovery of its development in different patients. It is refreshing to say that when I started this research in nanophotonics, I would not imagine its usage for potentially saving lives in the future!

CHAPTER 1.   INTRODUCTION

1.1   Creating Nanodevices from Nanostructures

The field of nanophotonics has been the subject of extensive expansion due to the unique capabilities of photonic nanostructures to control the propagation of EM waves. Owing to their constituent nanoscale features, which spectrally, spatially, and even temporally manipulate the optical state of the EM wave, nanophotonic devices extend all the functionalities realized by conventional optical devices in much smaller footprints. Combined with the advances in nanofabrication technologies, these nanostructures have been used to demonstrate devices with enormous potential for groundbreaking technologies addressing significant challenges in state-of-the-art applications, such as optical communications [1], signal processing [2], biosensing [3], energy harvesting [4], and imaging [5], to name a few. As an example, newly emerged metasurfaces [6] (MSs), two-dimensional planar structures comprising of densely arranged periodic/aperiodic arrays of well-engineered dielectric or plasmonic inclusions, offer profound control of the EM wave dynamics including amplitude, phase, polarization, and frequency in the subwavelength regime.

In recent decades, the advancement of fabrication capabilities has enabled researchers and engineers to create optical devices with geometries smaller than the wavelength of light (i.e., sub-wavelength structures). These structures open up a new range of optical possibilities that are of great interest but are often beyond the intuition of current engineering. Finding the optimum geometry and material for such nanostructures for the desired response is mainly limited to guesswork and computationally intense simulations

of Maxwell's equations. Researchers have been applying machine learning (ML) and deep learning (DL) to improve the inverse design process of nanostructures for specific optical responses within the past few years.

1.2 21st Century Challenges in Designing Complex Photonics Nanostructures

Systematic realization of mature optical functionalities using complex nanostructures requires significant knowledge about nanostructure features' influence on the propagation of EM waves, which currently can only be found using cumbersome numerical calculations. Besides, existing optimization approaches for EM nanostructures rely on significant iterations to get to a target device from an initial guess. Even by allocating unique computational resources, such time-consuming techniques are not guaranteed to reach the global optimum. Also, the methods do not provide much intuitive understanding of wave propagation dynamics inside these nanostructures unless a broad set of simulations is performed. Thus, developing new efficient approaches for rapid, accurate, and detailed analysis, design, and optimization of EM nanostructures is urgently needed and long overdue.

Early efforts were directed at using simple DL techniques to aid the forward problem, i.e., mapping design parameters of a nanostructure to its corresponding spectral response with NNs [7]. The trained networks approximate computationally intensive simulation software, allowing for much quicker design iterations at the cost of decreased accuracy. However, solving the inverse problem directly, providing a set of design parameters that results in a specific response, is of interest. This problem is much more challenging than

the forward problem because it is a non-unique function, where multiple design parameter combinations can yield identical optical responses. These parameter combinations include design choices such as the material, geometry type (layered structure, nanospheres, and repeating patterns), and the design geometry values. This creates a large search space with areas of redundancy when designing for a specific response, and there do not exist many broad techniques for trimming the search space and gaining an intuition about the problem.

In this thesis, we present a new series of physics-driven approaches based on AI to accelerate the designing of nanophotonic structures for achieving the desired response (i.e., reflection spectra of light in a specific band) while learning the underlying behaviors light-matter interaction.

1.3   Organization of Thesis

The thesis consists of six chapters. The introduction chapter is followed by the fundamental concepts and theoretical backgrounds of the inverse design of nanophotonic structures. This chapter discusses the conventional techniques for designing nanostructures and the main challenges in inverse designing nanostructures (i.e., non-uniqueness challenge and infeasibility challenge). In chapter three, I present the developed techniques for alleviating non-uniqueness challenges. Chapter four is dedicated to introducing a new method for studying the feasibility of having an optical response by bounding the latent response space. In the fifth chapter, I present a series of techniques based on the intelligent aspect of AI for knowledge discovery in nanophotonics. In this section, we study the role of design parameters in forming the response, introduce physics-driven manifold learning

approaches, and analyze the sensitivity of different designs. In the last chapter, I present a

summary of the contribution to the field and discuss the potential impactful next steps.

CHAPTER 2.   FUNDAMENTAL CONCEPTS AND

THEORETICAL BACKGROUNDS

This chapter summarizes the prior research on the inverse design of the nanophotonic structure and the role of AI in nanophotonics. The first part is an overview of the three primary challenges in designing complex nanostructures, the curse of dimensionality, non-unique solutions, and the existence of the solution. It is followed by a review of conventional approaches for tackling the challenges and the role of conventional AI techniques to accelerate designing nanodevices. This part also depicts the enormous potential impact of AI for investigating light-matter interaction in intricate scenarios.

2.1   Design and Optimization of Nanophotonics Structures

The widely used techniques for designing and optimizing nanostructures can be divided into two categories: 1) algorithms that rely on a random initial guess and iterative search [8-14] (e.g., a cycle of trial and error). These categories include brute force methods, evolutionary techniques, and algorithms that rely on cyclic trial and error. Such algorithms are customized for a specific design, i.e., for any arbitrary design problem. All the steps must be redone to find the suboptimal structure; 2) algorithms employing AI-based methods to optimize nanostructures' geometry [15-34]. While being more reliable in providing global optimum designs, such data-driven algorithms require a significant amount of training instances to be practical for real-world applications. Both approaches' enormous computational cost hinders their utilization for providing a detailed understanding of the fundamental properties of wave propagation in nanostructures. The

former category requires extensive computation power. The latter relies on the initial condition (i.e., starting point) and, in most cases, ends up finding local minima in the optimization landscape. Adjoint optimization approaches [35] can be employed to form a more efficient version of cyclic search methods, but still, designing complex geometries requires extensive computation. This shortcoming becomes more crucial as the number of design parameters grows.

In contrast, AI-based techniques deal with modeling input-output relation for a particular class of nanostructures. These models mainly form a multi-objective optimization platform and more computationally efficient. But still, by increasing the number of design parameters and desired response features, the methods struggle with convergence and end up with locally optimum nanostructures.

2.1.1   Curse of Dimensionality

One of the other challenges in using NN for designing nanostructures is dealing with a broad array of responses, so-called the curse of dimensionality [35] (its phase and amplitude define, i.e., each spectrum over the desired wavelength). In a typical design problem, to fully represent optical features, the spectral responses should be sampled spatially in small regions. Spectrally, it should be sampled with a spectral resolution more petite than the wavelength. This can result in thousands of samples just for a single spectrum. This number could even rise if the EM nanostructure provides sharp responses. Furthermore, to find the optimum nanostructure, the geometry should be defined with more design parameters. This leads to having a design problem with vast arrays of inputs and output. With data generation limitations (i.e., using EM simulation software for generating

each simulation is time-consuming), training a NN for mapping input to output is difficult. The trained network tends to memorize the relation rather than learning it.

2.1.2   Non-uniqueness Challenge

The non-uniqueness issue is one of the main challenges in using NN for inverse design, as conventional NNs are many-to-one models. Typically, in an inverse design problem there more than one set of design parameters that could provide the desired response. Modelling such one-to-many relation is relatively complex as in different part of the optimization landscape, we may have a different number of solutions for each selected feature (e.g., zero solution in a region and multiple solutions in the other region for the desired response but another desired response multiple solutions in the former region and zero solution in the latter region).

2.1.3   Feasibility of Optical Responses in Nanophotonic Structures

Despite extensive achievements in photonic nanostructures' inverse design, setting general constraints (e.g., material and fabrication constraints) make some desired responses fundamentally unachievable. This can cause significant issues in the convergence of design algorithms. For example, let's assume the desired response has a resonance in a specific frequency band, but the structure cannot provide such a resonance by any means. As a result, no design parameters exist corresponding to the desired behavior. Therefore, it is of great importance to determine whether finding design parameters for a class of structure (e.g., the unit cell of nano-rods) to achieve the desired response (by some acceptable error) is even possible or not.

2.2   Artificial Intelligence Meets Nanophotonics

Recently, AI-based design approaches combined with an efficient exhaustive cyclic search [27-28] have been implemented for designing nanostructures. Different methods to date mainly rely on training NNs using a set of design and response data (i.e., training set) gathered from EM simulation software to model input-output relation of optical nanostructures, then use the trained NN to solve the design problem.

Despite the progress in the AI-based design area, the current techniques primarily focus on modeling design problems with a smooth optimization landscape with almost one-to-one relation between design space and response space (i.e., a single set of design parameters exists for each spectrum). Different reported approaches to date primarily rely on training a NN (see Fig.1a) using the response of a set of devices (found by numerical simulations) and using the trained NN to solve the inverse design problem. Despite impressive progress in this area, the reported solutions mostly focus on solving simple problems with a reasonably smooth optimization landscape that have a one-to-one mapping of the design space to the response space (i.e., given response can be obtained by only a single set of design parameters) as shown in Fig 1b), where a vector of device response ($\overline{r\iota}$) is achieved by a unique vector of design parameters ($\overline{d\iota}$). In typical problems, most of the input-output relations do not have unique conditions. Figure 1c shows the optimization landscape of a more general problem in which the one-to-one relation between design and parameters and the output response parameters does not exist. As A result, trying to model a non-unique relation with a one-to-one model causes a convergence issue and leads to an invalid model. Efforts on turning a non-unique problem into a one-to-one problem by removing part of the dataset do not practically solve the case as the relation is still not one-

to-one. This can result in convergence issues for the NN used for optimization (finding design parameters for a given desired optical response). Efforts on converting the problem to a one-to-one mapping by removing some training datasets (see Fig. 1c) do not essentially help in solving the problem as most of the design space is not covered by these training datasets. Such approaches just smooth out the training data and fit a strictly ascending/descending to it. In another report, a tandem network is used to solve the challenge [15]. The technique relies on first training a NN to relate design space and response space, cascade it as a pre-trained NN (i.e., tandem network) with another network that links design space and response space, and then train the whole network. Since feed-forward NNs can provide multiple sets of output for a single set of inputs, the technique still cannot address the non-uniqueness issue. Another notable approach is based on using generative adversarial networks (GANs) to solve the inverse design problem. This technique is built on training a network to solve the forward problem with zero error and use it to generate ground truth data in each iteration. Training such a forward-problem-solver network with close to zero error in a general design problem is a significant challenge and may require excessive computational resources. Considering this challenge, by using such an accurate model, one could use it as a stand-alone tool for design, and it questions the necessitate of using the GAN-based design technique. In the reported design problem, each desired output needs extensive computation, which may reduce the value of using GAN if a perfect forward problem exists. The success of such techniques highly depends on the complexity of the problem and selection of the design parameters in the one-to-one region (outside the dead-zones in Fig. 1d) to converge acceptable answers.

More recently, new series of conditional GAN-based techniques has been used to solve the inverse design problem [24-27]. However, the techniques can provide a better comparison to trial approach errors. In essence, it can be considered as a variation of cyclic search, and the resulting output does not necessarily provide a viable design for the desired response.
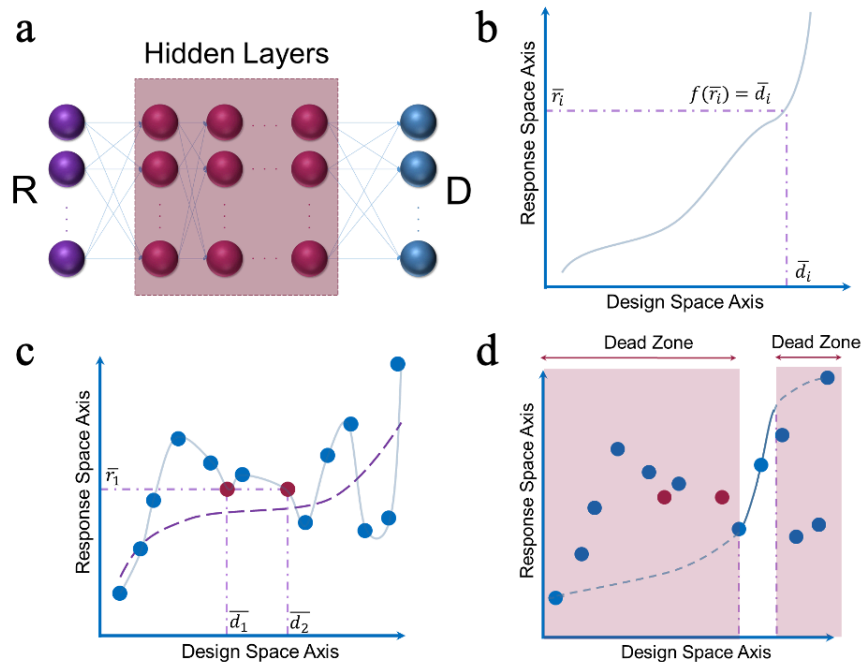
Figure 1 (a) A feed-forward NN for design and analysis of EM nanostructures; D and R represent design and response parameters, respectively. (b) Representation of a one-to-one design landscape as the most straightforward class of problems for the solution with the NN in a. (c) Representation of a general (non-one-to-one or many-to-one) design manifold. Red dots represent instances with the same response features obtained with different sets of design parameters. The light-blue curve demonstrates the original design manifold, while the dashed line shows the estimated one obtained

with conventional methods for solving the one-to-one problem (e.g., the NN in a). (d) Representation of the same design manifold as in c with a solution obtained by just training the NN in a for some intrinsically one-to-one region (outside the dead-zones); the non-optimal extrapolated manifold for the dead-zones is highlighted by red color.

Our solution for solving the mentioned challenges [36,37] a resolution to the existing simulation challenges in both providing valuable intuitive understanding and the design/optimization of the EM nanostructures by 1) extensively reducing the dimensionality of the problem using DL-based and AI-based approaches, and 2) using the unique features of ANNs for the analysis and design/optimization of the problem in the reduced space. The resulting simulation tool can take preliminary information to enhance any given feature (e.g., insensitivity to fabrication imperfections) throughout the process. It also provides a trade-off between the accepted error and the simulations' complexity (and time). Thus, it can obtain valuable information about the role of design parameters [38-40] on the overall device performance, get detailed information about a specific feature of the device, or design an optimum device for any given functionality.

CHAPTER 3. OVERCOMING THE NONUNIUNIQUENESS CHALLENGE WITH HIGH COMPUTATION COMPLEXITY

One of the main challenges in designing the desired nanostructure is the extensive computational complexity that EM simulation software imposes on the algorithm's total complexity. To alleviate this issue, I developed a series of DR-based techniques to reduce the computation cost while preserving sufficient information for studying/solving the design problem. Due to the non-uniqueness challenge finding the optimum low-dimensional space to represent the input-output relation is challenging. This chapter represents the invented techniques for reducing the dimensionality and overcoming one of the main challenges is the inverse design, non-uniqueness challenge. First section represents the invented technique based on DR for the accelerating design of nanostructure. In the next section, by employing the DR-technique we simplify the design problem and study some nanophotonics design problems. In the third section, we extensively study the effectiveness of the DR on reducing the computation costs. In part 4, we employ mixture density networks (MDNs) to not only overcome the challenge of non-uniqueness but also provide multiple solution for each desired optical response/functionality. This chapter is followed by studying the sensitivity of the response against the variation of the design parameters and design inconsistencies (e.g., fabrication imperfection).

3.1 Reducing the Dimensionality of the Nanophotonic Design Problems

To address both the network-size and non-uniqueness challenges, I demonstrate a novel approach for designing complex nanostructures. The method is based on reducing

the dimensionality of both design space and response space through training artificial NNs, called autoencoders [42]. Once the dimensionality of these two domains is optimally reduced, the problem converts to a one-to-one problem in the latent space, which can be solved with less computational complexity.

3.1.1 *Reducing Dimensionality of the Response Space*

Figure 2 shows the design approach's schematic based on the design space's DR, assuming that the optimization landscape is non-unique. The original forward problem is illustrated by path 1 in Fig. 2, where each point in the design space corresponds to a point in the response space through a many-to-one relationship. A NN cannot be trained to inverse this relation, as explained above. This is the main complication in the design and optimization problem. In the proposed approach [36], we first use the DR technique to reduce the response space's dimensionality as much as possible while preserving the essential information.
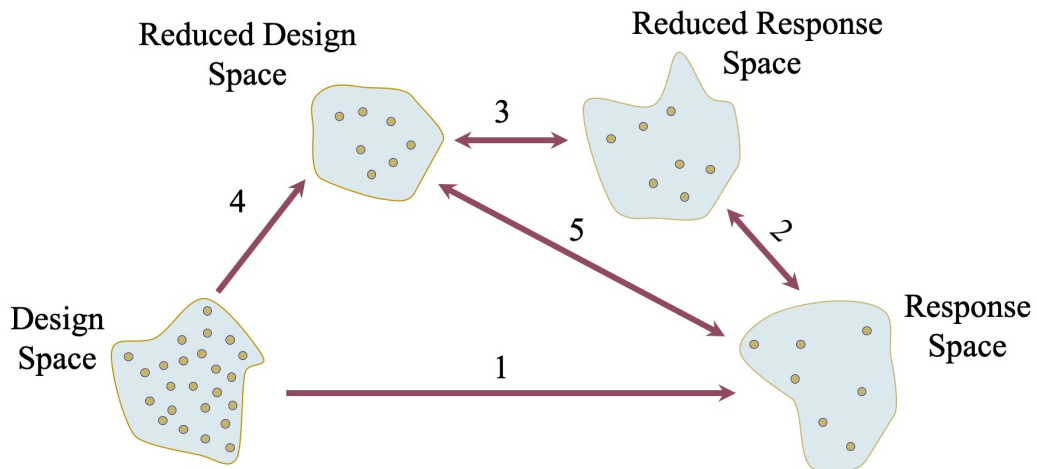
Figure 2 Applying the DR technique to the response and design space. In an optimal implementation, paths 1 and 4 are many-to-one, while routes 2, 3, and 5 are one-to-

one. The direction of the arrows indicated the ways that are easily achievable due to the one-to-one relation.

In the next step, we reduce the dimensionality of the design space as much as possible (see path 4 in Fig. 2). In this process, the design space's redundant nature is removed, resulting in a one-to-one relation between the reduced design and reduced response space (see path 3 in Fig. 2). After training the relevant DR mechanism, the relation between the original response space and the reduced design space will be one-to-one, and thus, one can simply invert the network. As the result, our design parameters are related to the original design parameters through a one-to-many relation analytically available through the training process (i.e., in the form of a formula with a series of nested Tanh(.) functions that model different nodes of the trained NN for the encoder part of the pseudo-encoder). Thus, we can find several design options by converting the resulting optimum reduced design parameters. At this stage, design constraints (e.g., fabrication imperfections, structure robustness, characterization limitations, etc.) can be taken into account to choose the final parameters.
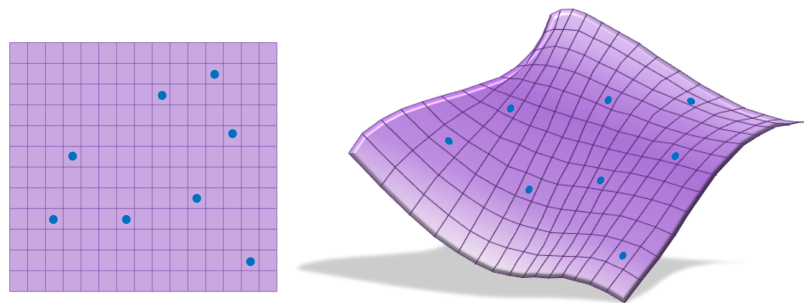
Figure 3 An example of the one-to-one DR. Each dot represents a point in the original space that corresponds to a point (shown by a dot) in the lower-dimensional space.

The heart of our approach is the effective implementation of the DR to efficiently reduce the dimensionality of both design and response space. Figure 3 shows a cartoon of 2D manifold in the 3D space and its corresponding representation in 2D space. However we have the one-to-one relation for reducing the dimensionality of the optical space, unfortunately we do not have that luxury in reducing the dimensionality of the design-response relation (i.e., design space). Several DR techniques have been developed in machine learning to facilitate classification, data visualization, and computation cost reduction. Among different approaches, principal component analysis, locally linear embedding (LLE) [43], and autoencoder are the most effective techniques. Considering these methods' features, we believe that autoencoder is the most suitable approach for solving inverse problems in general and designing EM nanostructures in particular.

Autoencoder consists of two parts, the encoder and the decoder (see Fig. 4), which can be defined as transitions $\emptyset$ and ψ, such that:

$$\emptyset, \psi = \operatorname*{again}_{\emptyset, \psi} \|X - (\emptyset o \psi)X\|^2 \tag{1}$$

The encoder takes the input $x \in R^n = X$ and maps it to $h \in R^p = \mathcal{F}$, which n and p are the dimensionality of the input space and latent space, respectively.
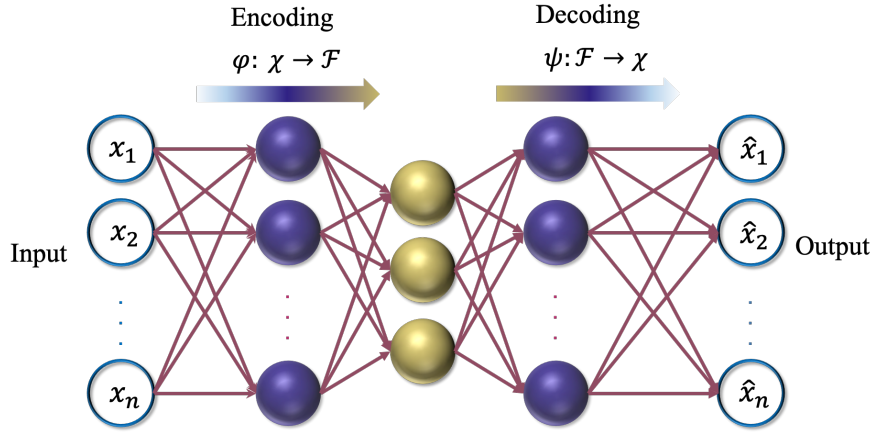
Figure 4 Schematic representation of an autoencoder architecture. Autoencoder is a type of NN which is used to code the unlabeled data.

To reduce the computational complexity, we first reduce the response space's dimensionality and train an autoencoder (see Fig. 4) using the dataset obtained from EM simulation software. We form a feed-forward NN to map the design space to the next step's reduced response space. Once the training is completed, we use the NN as a forward model to search over the reduced area to find the desired response (e.g., spectrum).

3.1.2 Pseudo-encoder: An Ideal Platform for Nanophotonic Structures

In the approach shown in Fig. 5, I invent the pseudo-encoder architecture that relates the original designs (i.e., $d \in R^m = D$) space to the reduced response space (i.e., $f \in R^p = \mathcal{F}$) as it is shown in Fig. 4. By training the pseudo-encoder to reach the bottleneck layer's minimum size, we reach the reduced design space (i.e., $g \in k = G$).
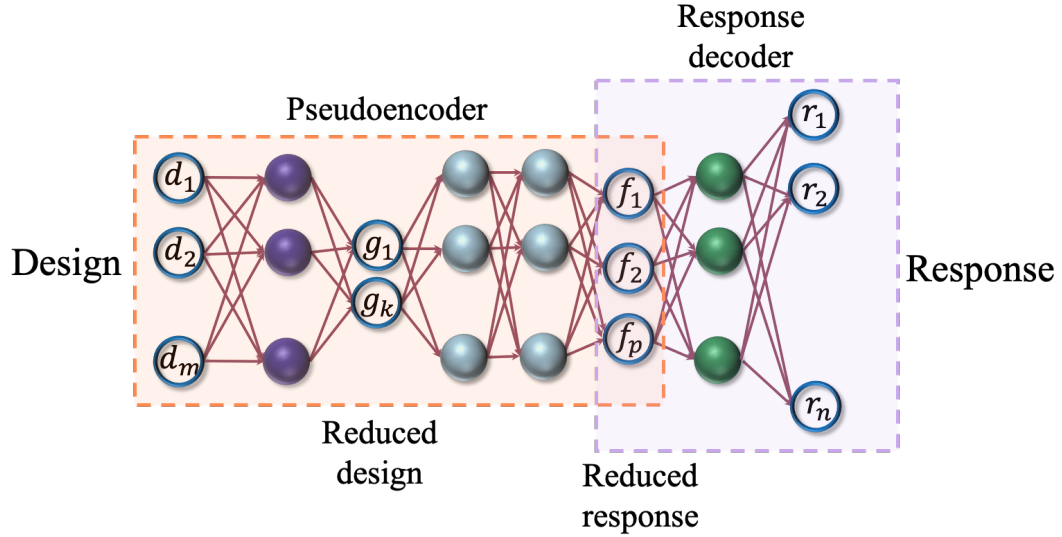
Figure 5 Architecture of a pseudo-encoder, which relates the original design space to the reduced response space while reducing the design space's dimensionality. The response decoder part retrieves the actual responses from the reduced response.

Once the DR of the two spaces is complete, I form a NN by cascading the pseudo-encoder and the pre-trained response decoder (see Fig. 5) to create a full forward modeler.

3.2 Deep Neural Network for Modeling Forward Design Problem

In this section, by applying the developed technique, we first reduce the dimensionality of the design problem and use a comprehensive DL-based tool to analyze and design the nanophotonic structures.

3.2.1 A Comprehensive Deep Learning Model for the Forward Problem: Analysis

To show the DL model's applicability, we consider four different generic photonic nanostructures design problems (see Fig. 6). For all nanostructures, first, I randomly select

design parameters in a feasible range, excite the structures with light, and measure the reflectance using EM simulation software to obtain the training data set. In the next step, I use the training data to train an autoencoder to study the DR technique's accuracy. Figures 6a, b, c, and d show the comparison of the actual reflectance spectrum and the reconstructed data using the autoencoder for different dimensionalities (i.e., p = 20, 10, 5, and 2) for nanostructures in Figure 6a, b, c, and d, respectively. The spectrum can be encoded from 200-dimensional space to 5-dimensional space with negligible error for all problems.
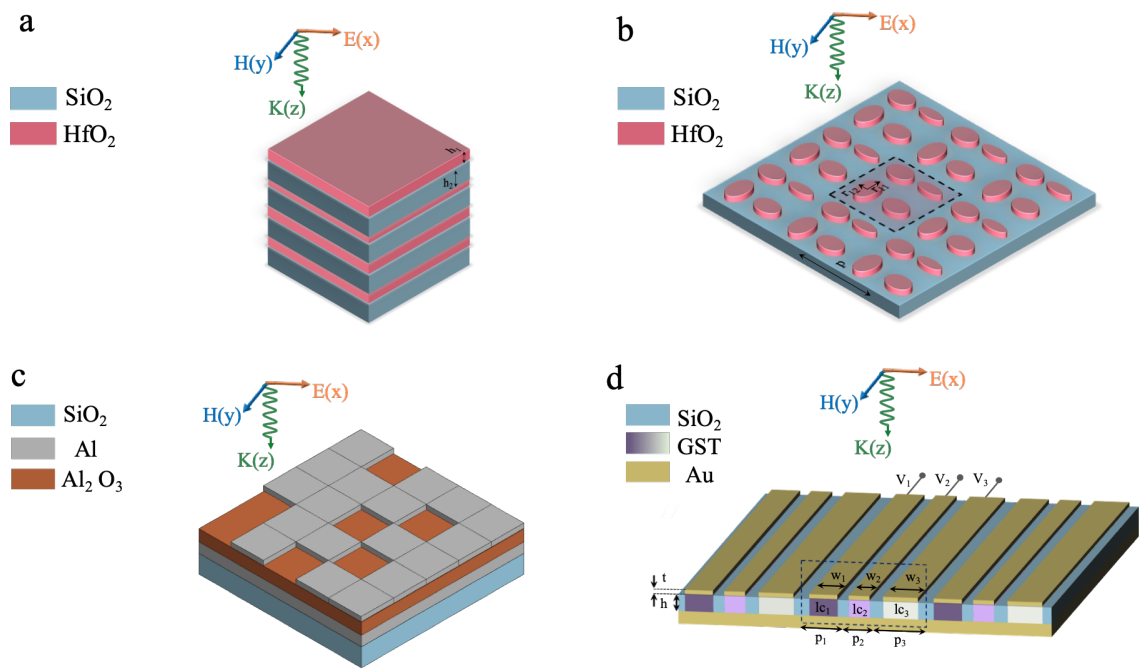
Figure 6 Representation of four classes of nanophotonic structures. (a) Multilayer nanostructures [44-45] are made of SiO₂ and HfO₂. The thickness of each layer (i.e., h_i) is a design parameter. (b) Dielectric structure [46] is made of SiO₂ and HfO₂. The design parameters are periodicity (i.e., p) and radii of the ellipsoids (i.e., r_{ij}). (c) Binary

plasmonic MS [47-49] made of SiO₂, Al, and Al₂O₃. Each binary pattern forms a design instance. (d) A periodic MS with reconfigurable reflectivity [36] formed by a periodic array of Au, GST, and Al₂O₃. Widths (i.e., w_i), pitches (i.e., p_i), crystallization levels (i.e., lc_i), and GST height (i.e., h) are design parameters.

Reducing the dimensionality of the design and response spaces considerably lessens the computation complexity as the resulting problem's dimension becomes orders of magnitudes less than the original problem (e.g., 3 to 5 instead of 20 to 200). Moreover, training the pseudo-encoder that relates the design space to the reduced response space (see Fig. 7) required much less computation than the NN that bonds the design space to the response space.

3.2.2 *Inverting the Deep Learning Algorithm for Non-unique Problems: Design*

Also, to decrease the computation complexity, I invent a double step DR [36] technique to solve the inverse problem. In the first step, I invert part of the NN, which relates the reduced design space to response space. This is easily achievable as the relation between these two spaces is one-to-one. (see path 5 in Fig. 2). Then, relate the reduced design space to the design space. This can be done by searching over the feasible design parameters with an order of magnitude lower computation. I use analytic relation between the original and the reduced design spaces to thoroughly explore the actual design space to find the points corresponding to the desired point in the reduced design space.
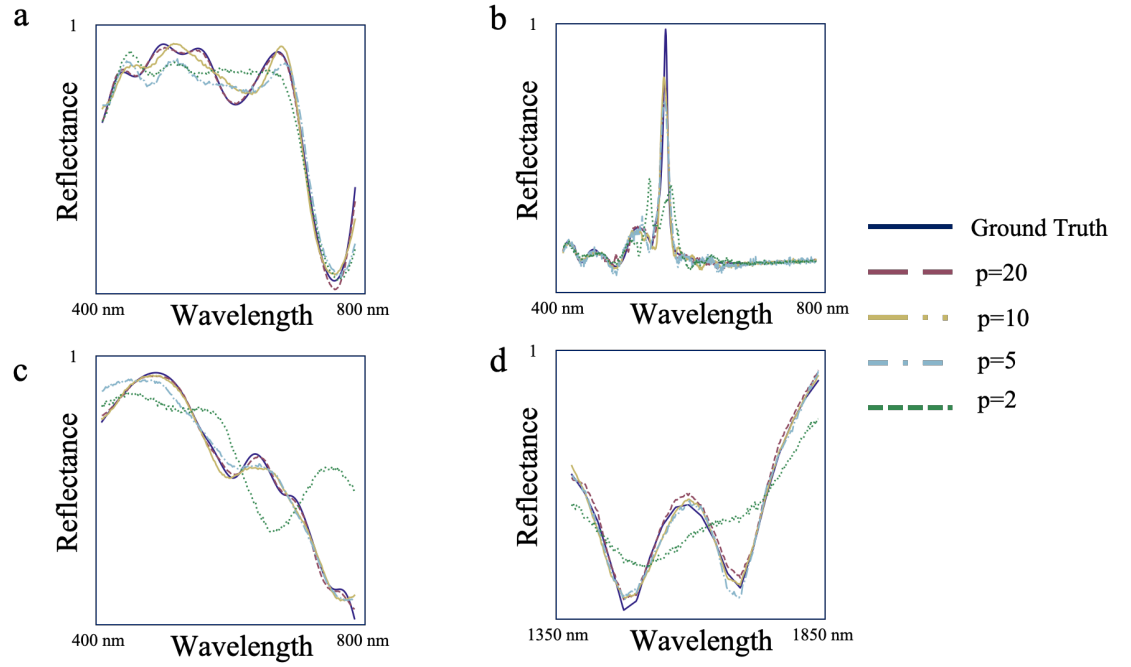
Figure 7 Reconstructing the response of the nanostructures in (a) Fig. 6a, (b) Fig. 6b, (c) Fig. 6c, and (d) Fig. 6d after DR as a function of dimensionality of the reduced response space.

To show the design approach's applicability, in a collaboration with our groupmate, we consider a class of design problems to implement a reconfigurable metasurface enabling optical modulation, as shown in Fig. 6d. The nanostructure has ten design parameters (i.e., w_1, w_2, w_3, p_1, p_2, p_3, h, l_{c1}, l_{c2}, and l_{c3}). As an exciting functionality, we are interested in the amplitude modulation of the incident light at λ = 1600 nm with a considerable bandwidth around the central wavelength. We use the autoencoder and the pseudo-encoder to reduce the dimensionality of the problem from 10×200 to 5×10.

Figure 8 shows the performance of the DR approach for the nanostructure in Fig. 6d for five different random set of design parameters. The left panel represent the results

of reducing dimensionality of the response and the right panel shows the results of reducing

the dimensionality of the design. These results support the effectiveness of the DR

technique that is presented in this chapter.

d

e
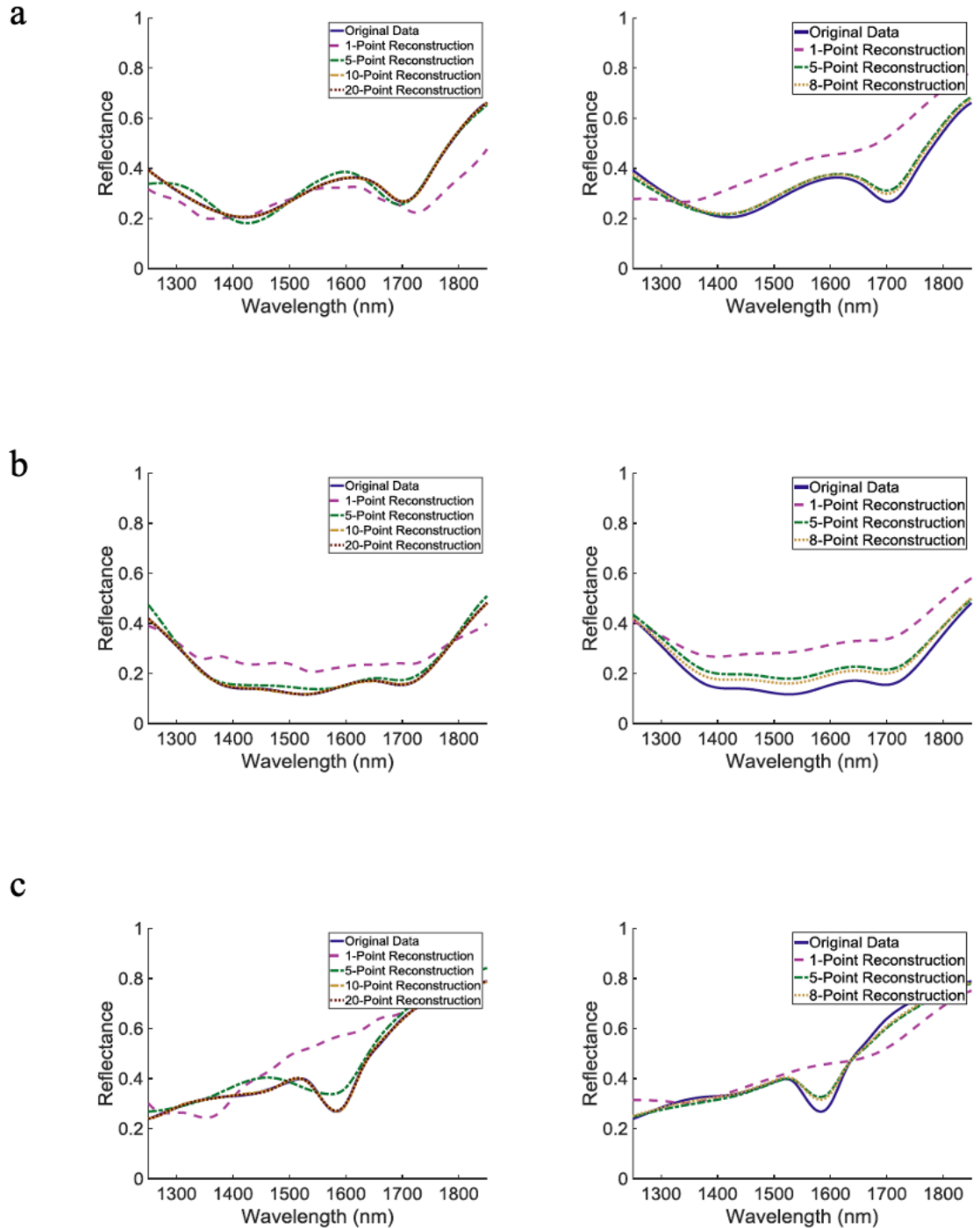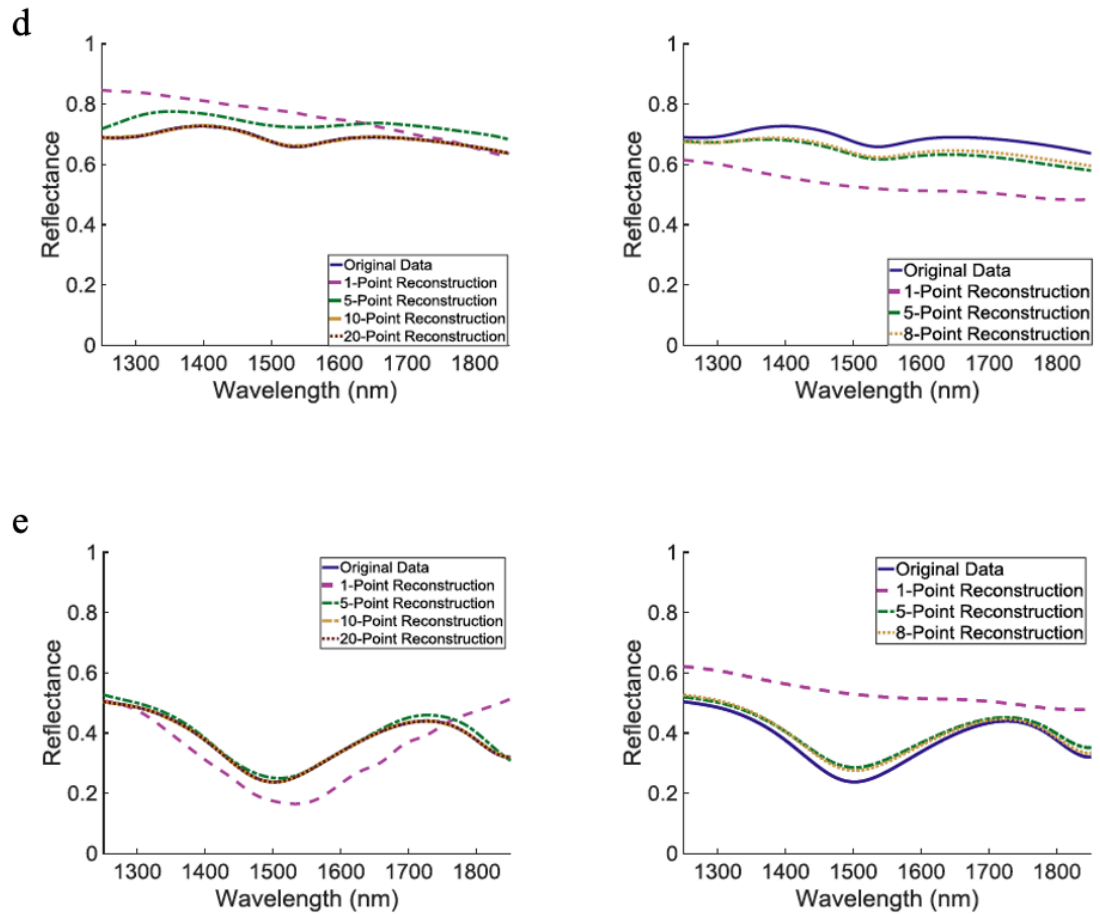
Figure 8 (a)-(e) the reconstructed response of the nanostructure in Fig. 6 of the main text after DR of the response space (left) and both spaces (right) for different dimensionality of the reduced response space (left) and the reduced design space (right, with dimensionality of the reduced response space being 10 for all cases) for five different test instances (not used in training).

Figure 9 shows the results for designing a perfect light absorber for operation in the 1500-1700 nm wavelength range using the structure in Fig. 6d. The desired response is zero reflectivity over the entire operating bandwidth. The overall mean squared error

(MSE) for the optimal structure response (i.e., D_1) in Fig. 8 is 0.0147. The reflectance for the three other sub-optimal designs (i.e., D_2, D_3, D_4) with considerably different design parameters are also shown in Table 1.

Table 1 The design parameters and the resulting MSE for the optimal design and three good designs for the structure in Fig. 6d to achieve maximum absorption in the 1500-1700nm wavelength region. h, w_i , and pi {i=1,2,3} are in nm.

Design	h	l_{c1}	l_{c2}	l_{c3}	P1	P2	P3	W1	W2	W3	MSE
D_1	190	0.5	0.6	0.7	650	650	550	350	500	200	0.0147
D_2	190	0	0.2	0.8	650	650	350	450	250	250	0.0149
D_3	190	0.5	0.1	0.7	650	450	450	200	350	300	0.0152
D_4	190	0.3	0.6	0.8	650	550	550	250	300	450	0.0172

Figure 9 (a) Achieved spectral responses for the full absorption in the 1500-1700 nm wavelength range [36]. Responses of the optimal (D_1) and three other reasonably good, designed structures (D_1, D_2, D_3) to achieve maximum absorption in the 1500-

1700nm wavelength region (shown by the shaded rectangle) is depicted. The dotted blue line indicates the reflectance spectrum in the off-state (D_{off}).

3.3 Analyzing the Effectiveness of Dimensionality Reduction in Reducing the Computation Complexity of the Nanophotonics Design Problems

In this part, we present a deep learning-based method using NNs for inverse design of photonic nanostructures. We show that by using DR in both the design and the response spaces, the computational complexity [44] of the inverse design algorithm is considerably reduced. As a proof of concept, we apply this method to design multilayer thin-film structures composed of consecutive layers of two different dielectrics and compare the results using our techniques to those using conventional NNs.

3.3.1 Analysing the Computation Complexity of the Nanophotonic Inverse Design Problems

The invented technique is a systematic approach for the inverse design of non-unique nanophotonic structures based on reducing the dimensionality of the design and response spaces (DS and RS, respectively). We show that by solving the inverse design problem using the reduced design space (RDS) and the reduced response space (RRS), the computation requirements are reduced by orders of magnitude. The inverse-design approach is based on dividing the large overall non-unique (and thus, non-invertible) problem into a combination of a large invertible problem (between the response space and the RDS) and a small non-invertible problem (between the RDS and the original design space). To demonstrate this approach's unique features, we apply this method to design

standard multi-layer thin-film structures (See Fig.6a) composed of consecutive layers of silica (SiO$_2$) and titania (TiO$_2$). Our detailed comparison with the alternative approach based on training a conventional NN without DR shows an improvement by 2-3 orders of magnitude in the number of floating-point operations per second (FLOPS) without imposing a significant error.

Feedforward NN (FNN) that is used as the baseline for comparison of the computational performance of different approaches. Considering the design space $X \in \mathbb{R}^d$ and the response space $Y \in \mathbb{R}^r$, the FNN is trained to learn the mapping $F: X \rightarrow Y$ with minimal MSE between the predicted and simulated responses. Then, for a desired response $Y \in y^r$ the trained FNN will be used to search over the design space and find the optimum set of design parameters so that:

$$x^* = \arg\max Loss(y, y^*), \ x \in X \qquad (2)$$

where $y = F(x)$, $y^* = F(x^*)$, and $Loss(y, y^*)$ is considered as the MSE (i.e., $||y - y^\wedge *||$). Although the FNN is significantly faster than an EM simulation software for searching over the design space, the computation will increase as the number of the design parameters and the complexity of the structure increases (since a network with more nodes and layers needs to be trained). This shortcoming is addressed in this section by employing DR. The first step in our DR-based design approach is to reduce the dimensionality of the response space using an autoencoder. Due to the high redundancy in the response of a photonic nanostructure, the dimensionality of the response space can be reduced extensively without significant error. The optimum dimensionality of the RRS can be found using an adhoc method by changing the size of the bottleneck layer in Fig. 4). Once the autoencoder is

trained, we can reduce the dimensionality of any given response using the encoder. Next, we consider the pseudo-encoder network (Fig. 5) to reduce the dimensionality of the DS. The first part of the network (i.e., DS-to-RDS) maps the DS into the RDS. Then the RDS-to-RRS network maps the RDS to the RRS. Finally, using the decoder part of the trained autoencoder, the RRS will be mapped to the original RS. During the training, the MSE will be minimized over the original RS (note that the weights of the decoder part in are fixed by the trained autoencoder for the response space.

As discussed in previous sections, the relation between the RDS and the RS is one-to-one and can be inverted, while the mapping between the design space and the RDS is not one-to one. To find the inverse relation, we freeze the weights of the RDS-to-RRS network and concatenate it with a similar network from RRS to the RDS and training the RRS-to-RDS to find optimal parameters. Thus, the inverse design approach for a desired response is composed of two steps. First, we use the inverted relation between the RS and the RDS to map the desired response into a single point in the RDS. To simplify this inversion, we use the autoencoder to map the desired response to a point in the RRS, which will then be mapped to the corresponding point in the RDS using a trained network between the RRS and RDS. Secondly, we use the trained DS-to-RDS part of the network in to search over the design space and find the optimum set(s) of design parameters that map to the target point in the RDS. By using this two-step process, we considerably reduce the computation as the exhaustive search is performed over the smallest part of the pseudo-encoder, rather than the entire NN between the DS and the RS as in the conventional NN-based model.

3.3.2   Proof of Concept: Analysing the Computation Complexity of a Thin-film Design

Problem

To show the efficacy of our method, we perform the inverse design of an 8-layer and a 20-layer thin-film structure shown in Fig. 6a. These structures are composed of consecutive layers of SiO_2 and TiO_2, and the design parameters are the heights of different layers ($h_i \in [30, 70]\, nm$) while the responses are 200 samples of the transmission spectrum from 300 to 750 THz [44]. This results in the dimensionalities of 8 and 20 for the DS for the first and second structures, respectively, and 200 for the RS. For comparison purposes, we also train a conventional NN and use it for inverse design of similar structures. The inverse design in this case is performed through an exhaustive search between the DS and the RS using the FNN. For each structure, we generate 50,000 sets of random design parameters and find the corresponding responses using the transfer matrix approach, implemented in Python. We use 80% percent of the dataset for training the algorithm and the remaining 20% for testing it. We compare the FLOPS and the normalized MSE (NMSE) for the FNN and the PE over the 8-layer and the 20-layer datasets.

To investigate the existence of non-uniqueness in our dataset, we produce sets of design parameters with nearly identical optical spectrums with an accelerated brute force approach. We use the trained FNN to find three sets of design parameters that result in the minimum MSE between the calculated response and the desired response. The FNN used for the 8-layer structure has 4 hidden layers, each with 100 nodes and tangent hyperbolic (i.e., tanh) as the activation function. After training, the average NMSE over the test set for this network is 1.3×10^{-5} with 102,200 FLOPS for calculating the response of each test instance. Figure 3 shows the result of this investigation for an 8-layer structure. Figure 10b

shows very similar responses for the three selected structures despite major differences between their design parameters (see Fig. 10a). A similar observation is obtained for the case of 20-layer structures with a slight increase of error. This clearly indicates the presence of sets of non-unique design parameters that need to be addressed during inverse design.
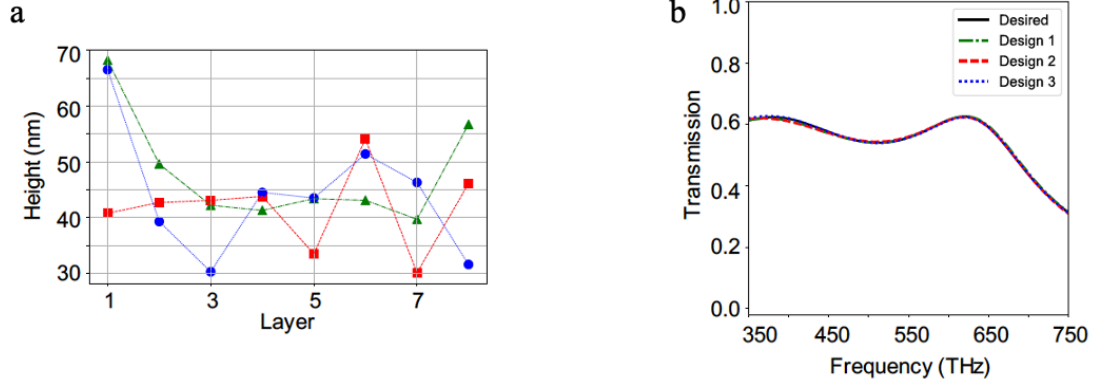
Figure 10 (a) The three best sets of design parameters (i.e., the heights of different layers) for the 8-layer structure of Fig. 6a for achieving the desired response and (b) their corresponding transmission responses. The NMSE between the desired response and the responses of the Design 1, Design 2, and Design 3 structures are 4.2×10^{-5}, 4.7×10^{-5}, and 3.8×10^{-5}, respectively.

To reduce the dimensionality of the design and response spaces for the 8-layer structure, we first train the AE using different numbers of nodes for the bottleneck layer to find the optimum dimensionality of the RRS. Our results show that with a 9-layer autoencoder (4 layers for the encoder, four layers for the decoder, and one bottleneck layer), the best dimensionality of the RRS is 12 with a NMSE of 2.2×10^{-6} with 200, 100, 50, 30, 12, 30, 50, 100, and 200 neurons in each layer, respectively. The activation

functions of all intermediate layers are tanh($\cdot$) with no activation functions in the input and output layers. We will then use a similar ad-hoc approach to find the best dimensionality for the RDS by training the pseudo-encoder part with a varying size of the bottleneck layer. We find that the optimum dimensionality of the RDS to be three using a pseudo-encoder with a total of 8 layers with 8, 5, 5, 3, 100, 50, 30, and 12 nodes in consecutive layers. The average NMSE of the trained PE over the test set is 7.6×10^{-4} with 14,685 FLOPS (for connecting the DS to the RRS). However, the mapping between the DS and the RDS, which will be needed for the exhaustive search in the inverse design, is performed using the DS-to-RDS network with only 173 FLOPS, which is smaller than the number of FLOPS needed for the FNN by a factor of ~600. Note that in practice, it is preferred to use a random search (rather than an exhaustive search) for finding the best designs. Nevertheless, the advantage of the DR approach over the FNN remains the same as it applies to every step of the search process. The FNN for the 20-layer structure has 4 hidden layers, each with 300 nodes and tangent hyperbolic (i.e., tanh) as the activation function. This NMSE over the test set for this network is 1.2×10^{-3} with 673,400 FLOPS for each test instance. Using a similar approach, the dimensionality of the response space for the 2-layer structure is reduced to 20 with an average NMSE of 6.2×10^{-5} using a 9-layer AE with 200, 100, 50, 30, 20, 30, 50, 100, and 200 neurons in each layer, respectively. Figure 11a shows the variation of the MSE of the autoencoder with the dimensionality of the RRS, and Fig. 11b compares the corresponding responses in the autoencoder with the original response. The corresponding 8-layer pseudo-encoder for this case has layers of 20, 20, 10, 8, 100, 50, 30, and 20 nodes, with the optimum dimensionality of 8 for the RDS. The average NMSE of the pseudo-encoder over the test set is 1.1×10^{-2} with 17,398 FLOPS for the entire pseudo-encoder and

1,398 FLOPS for the DS-to-RDS network. This shows a computation advantage over the FNN by a factor of ~500. Figures 11a and 11b show the performance of our pseudo-encoder-based approach and the FNN for the inverse design of the 8-layer and the 20-layer structures, respectively. In both cases, the desired response was not used in training or testing. Our algorithm uses random search instead of exhaustive search to address the non-uniqueness issue. The results shown in Fig. 11 are the designs with the lowest NMSE. The NMSE between the desired (i.e., simulated) and the designed responses in Fig. 11a are 3.4 $\times$ 10^{-5} and 1.7 $\times$ 10^{-3} for the FNN and the pseudo-encoder approaches, respectively. The corresponding values of NMSE in Fig. 11b are 2 $\times$ 10^{-3} and 3.6 $\times$ 10^{-3} for the FNN and pseudo-encoder, respectively. The reported numbers are average numbers obtained in testing the algorithms for many designs in order to be good representatives of the performance of the two inverse design approaches.
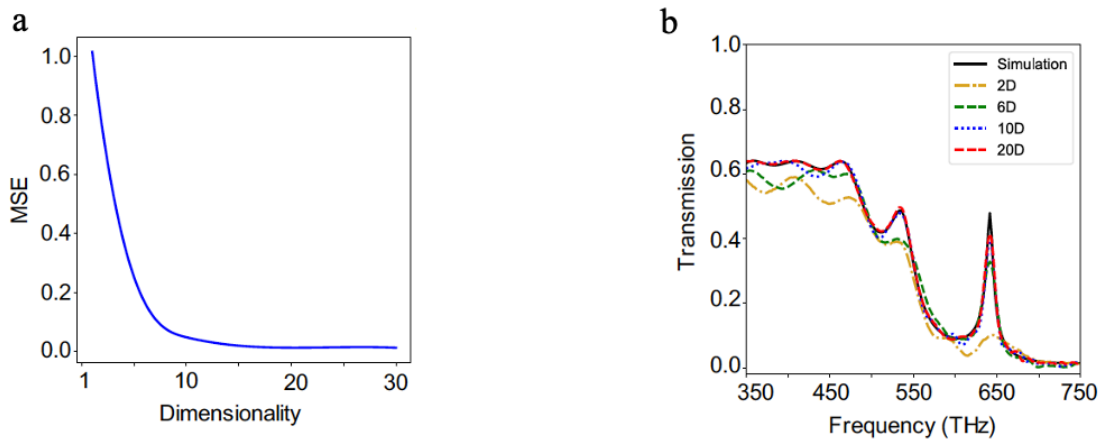
Figure 11 Finding the best dimensionality for the RRS. (a) The variation of the NMSE with the dimensionality of the RRS (i.e., the number of nodes in the bottleneck layer for a 20-layer structure in and the corresponding responses for different

autoencoders with different dimensionalities of the RRS along with the original simulated response.

Figure 11 shows the advantage of our pseudo-encoder-based technique in performing the inverse design of a multi-layer structure over the conventional NN-based approaches in achieving similar NMSEs with 2-3 orders of magnitude reduction in computation. This advantage becomes more important for complex nanostructures with many design parameters where the computation of the FNN algorithm becomes excessive. While the actual computation advantage of the pseudo-encoder-based approach depends on the nature of the problem on both design and response spaces, we expect the observed numbers in this paper to be good representatives of such an advantage.

It is important to note that the numbers of nodes in the layers of the PE after the bottleneck layer (i.e., the RDS-to-RRS network) do not affect the computation advantage of the pseudo-encoder in inverse design as the only part used for the final search is the DS-to RDS network. Nevertheless, it is important to optimize the dimensions of the RDS and RRS to ensure a one-to-one relation between the RDS and the RS to enable the simple inversion from the RS to the RDS. This is currently done by trying different dimensions for the RRS and the RDS. Future research should be performed to develop more rigorous approaches for finding such optimal dimensions.

While the pseudo-encoder-based approach is computationally favorable over the FNN during the inverse design phase, it requires more computation during the training phase since the pseudo-encoder requires training of two separate networks: the autoencoder for the DR of the RS, and the pseudo-encoder for that of the design space. However,

31

training is performed only once for all the inverse design attempts using a given photonic device architecture. Thus, the added training computation is not a major disadvantage of the pseudo-encoder-based approach. Although we considered thin-film structures with 20 layers in this paper, our dimensionality-reduction approach can be used to reduce the computation requirements for structures with any number of layers. The computation advantage of the approach will be even more for more complex structures, especially with careful optimization of the dimension of the latent space based on the acceptable reconstruction error. Note that there is a trade-off between the dimensionality of the latent space (and thus, the computation requirements) and the error in reconstruction of a given response by the autoencoder, as can be seen from Figures 12a and 12b.

A unique feature of the demonstrated approach is its generality and applicability for designing and investigating a variety of different nanophotonic structures for different applications, as long as the response features are covered in the training phase. This is in contrast to the conventional design approaches where the entire design process has to be repeated once the desired response changes (even slightly).
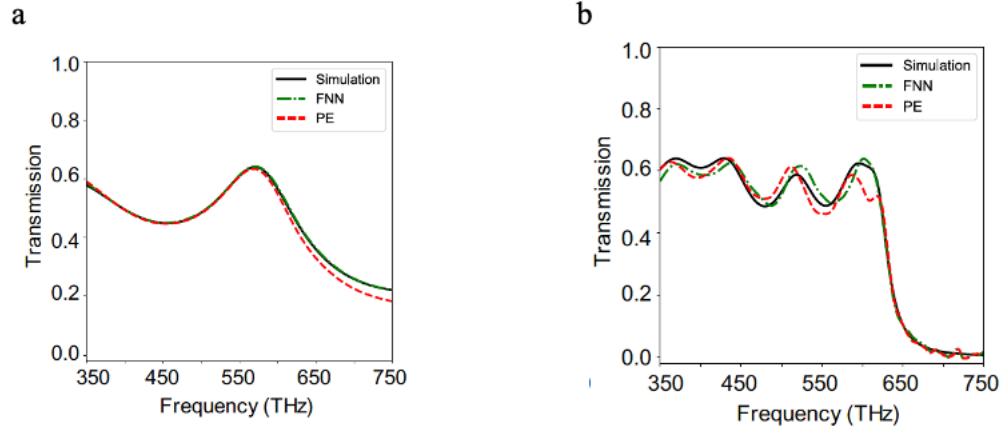
Figure 12 The desired and obtained responses (i.e., through inverse design) for the structure in Fig. 10 with (a) 8 layers and (b) 20 layers using the FNN and the pseudo-encoder. The deviation from the desired response represents the error in the designed structure.

3.4 Employing Mixture Density Networks to Overcome the Non-uniqueness Challenge

Here we present an algorithm using multiple MDNs [41] to first aid in reduction of design parameter search space, and then to suggest complete optical nanostructures based on desired optical responses. We then demonstrate this approach during inverse design of a multilayered metamaterial device based on desired spectral responses. We first reduce the design search space by providing material choices for the structure, and then use a suitable material to complete the inverse design process and suggest device geometries.

The methodology and trained networks guide design choices for a nanostructure based on a desired optical response and reduce the parameter search space to provide

33

insights about the design problem. To demonstrate the effectiveness of the proposed technique, we apply this method to a multilayer optical metasurface design problem. First, a trained network intuits information about material selection, and second, a network suggests layer heights to form a complete device proposal for any given desired optical response.

As a proof of concept, we apply the proposed technique to design a multilayer structure. The first step is verified by a reduced dimensionality representation of the spectral responses which shows visually a range of materials for a given response. The second step of the design process is verified by a forward solving NN that approximates the spectral responses of the complete designs.

In general, the goal of our proposed methodology is to first find a sweet spot for the ranges of design parameters which are capable of producing a desired optical response, and thus gain intuition about the design problem. Secondly, we wish to complete inverse design of an optical structure using this gained knowledge. We accomplish this with a MDN trained to capture the probability density of design parameters based on optical responses as input, and a secondary MDN to complete the outlined inverse design.

A MDN is a NN with a final layer consisting of parameters for creating a Gaussian mixture distribution. Instead of the network trying to learn one correct answer, it learns a probability density of possible solutions by training a mixture of normal Gaussian curves. The number of Gaussian distributions combined to form the total density function is the number of mixtures, and each mixture is represented by a mean (μ_i), a standard deviation

(σ_i), and a mixing coefficient (α_i). Equation (3) describes a Gaussian function used as the kernel for the mixtures, where **x** is the input given by the NN and **y** is the ground truth.

$$\phi_i\,(y|x) = 1/\sqrt{(2\pi\sigma_i(x)^2}\,\exp\,(-(\mu_i(x)-y)^2/2\sigma_i(x)^2) \tag{3}$$

Equation (4) describes the complete probability density function the network tries to learn. Note that the mixing coefficients add to 1.

$$p(y|x) = \sum_{i=1}^{m}\alpha_i(x)\phi_i(y|x) \tag{4}$$

MDNs are well suited to nanophotonics problems because of the non-uniqueness issue during design [36]. They can handle multiple correct answers in a training set for a given optical response, thus they can capture valid ranges for design parameters. If the ranges are distinct, then individual mixtures will be tuned to capture those search spaces. The range of values within each mixture is captured by the standard deviation of the mixture. In order to extract values for design and engineering purposes from the probability density function (PDF), several techniques can be used to sample the distribution. One approach is to randomly sample the distribution. Another approach is to take the mean of the constituent mixtures assuming a threshold for the mixing coefficient is above some value.

3.4.1   *Designing Multilayer Nanostructure Using Mixture Density Networks*

To show the effectiveness of this technique, we chose the task of designing 7-layer nanostructures (see Fig 6a) based on desired spectral responses. Two fictitious materials were chosen and alternated to form the layers. To simplify the model, the materials are

represented by only one of their design parameters, the relative permittivity ϵ_r. The odd layer material ϵ_r was held constant at 1.46 across all devices, and the even layer ϵ_r were uniformly sampled between 2.9 and 6.1 for a single device. The layer heights for the device were uniformly sampled between 100 nm and 200 nm. The data set to train this problem included 40,000 simulated devices and their corresponding spectral responses, generated using a modified MATLAB script originating from Umit's work [50], and randomly split up 70% for training, 10% validation, and 20% for testing. The output spectrum is the magnitude of EM reflection for frequencies between 450 THz and 750 THz (wavelength 400 - 666 nm), sampled over 200 evenly spaced points.

Next, we create the first MDN which includes 200, 60, 40, 10, 12 nodes at each layer, respectively. The input of the MDN corresponds to the spectral responses (200 samples of the reflection response) and the output of the network corresponds to 4 sets of mean, standard deviation, and mixing coefficients (total of 12 parameters). The hidden layers are fully connected and form a nonlinear mapping between the spectral response and the parameters that describe the final PDF. Figure 12b shows the probability density functions of the relative permittivity for the corresponding responses in Fig. 12a. Inspecting the PDF, we can determine ranges of materials capable of constructing devices with a given optical response.

After a range of values for ϵ_r is found, we train a new MDN to capture the relation between spectral responses combined with a chosen ϵ_r, and geometry parameters for our optical device, in this case layer heights. This MDN in essence tries to suggest layer heights for an optical device based on a given spectral response and the ϵ_r for the even layer material. This network architecture includes 201, 20, 40, 60, 60 nodes at each layer, where

36

200 is the combined input of spectral response and ϵ_r, and 60 represents the parameters for the PDF given an input. The MDN is trying to predict a 7D PDF because each representing the height of the structure, so with 4 mixes, we can calculate $4mix \times (7\mu/mix +7\sigma/mix +1\alpha/mix) = 60$ nodes. In order to generate device architectures, we sample our PDF at the means of the mixtures.

In order to verify our results, two additional networks are built. The first is an autoencoder to pair with the first MDN and better visualize the types of material available to a designer for a desired spectral response. Utilizing this deep NN, we compress the responses to a 2D latent space, by using the spectral responses for the devices as both input and output for the network and a bottleneck. The network architecture includes 200, 80, 40, 20, 10, 2, 10, 20, 40, 80, 200 nodes at each layer. The ϵ_r values used to generate each spectral response is kept handy to tag our responses compressed in the latent space. Figure 13c displays our sample spectra mapped to the latent space, along with many other samples that are colored based on their $_r$ value. It is clear that at each point in the latent space, a variety of colors can be found, thus confirming our hypothesis that a variety of materials can be used to generate such a response. Auto-encoding alone can provide similar function to our MDN but is prone to high error and is better suited to provide a qualitative compliment to the quantitative range the MDN supplies.
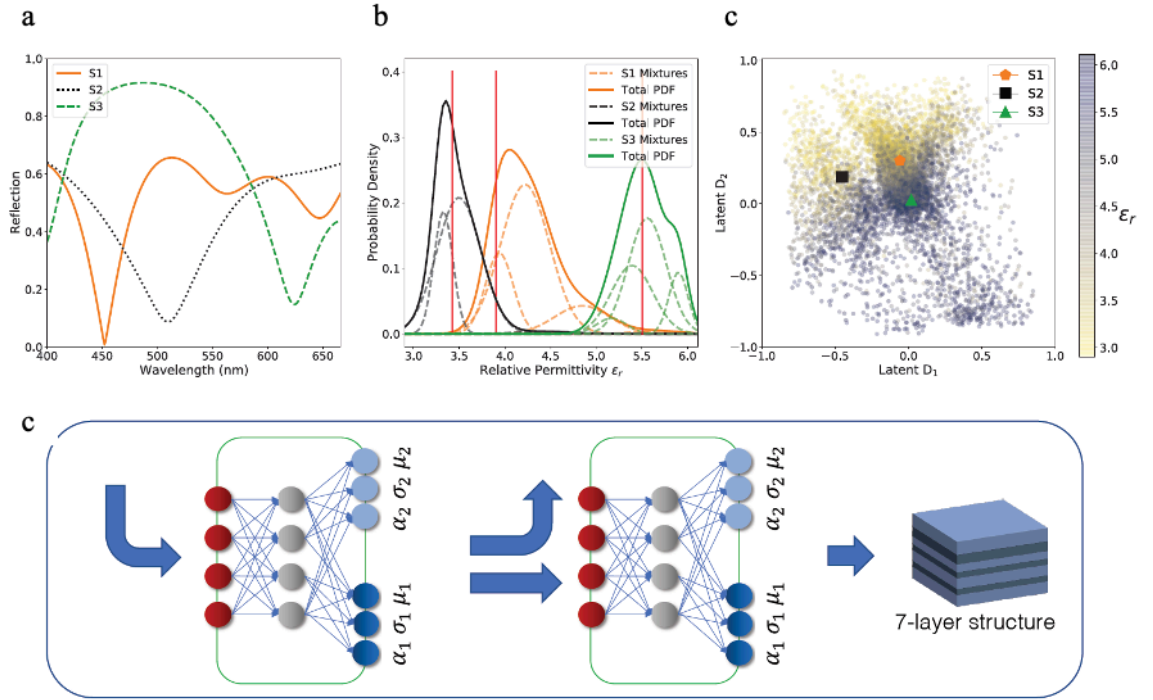
Figure 13 (a) Randomly selected spectral responses that act as filters for different target frequencies. (b) MDN for the spectral responses describing the range of materials that are capable of creating such a response. (c) The spectral responses encoded in a lower dimensional space, verifying the output of the first MDN. (d) Describes the two MDN design flow for designing a device. procedure, some additional optimization steps could be taken to fine tune a design based on the PDF.

Next, we model the input-output relation (i.e., design-response space) by training a feed forward NN. This network was employed to predict the corresponding spectrum for each set of design parameters (e.g., layer heights and ϵ_r). Figure 13a shows the effectiveness of this network in predicting the spectral response of a set of original design parameters (i.e., layer heights and ϵ_r). Figure 13b shows the same network validating designs suggested by the second MDN.

After training all the networks, we are able to implement our methodology shown in Figure 13d. First, we supply a desired spectral response (for testing, we randomly chosen from our test set), and find a PDF that describes material $_r$ values that may be used to generate such a response. This step can be verified by viewing the spectrum in the latent space. Upon inspecting the generated PDF, a clear range of possible materials can be compared to known materials to find a suitable match. For certain desired spectral responses, materials with the necessary properties cannot be supplied by the materials science community.

3.4.2   *Selecting the Optimum Material In a Design Problem*

Next, the selected material is supplied along with the same desired spectral response to the secondary MDN. This generates options for layer heights (see Fig. 14). If a different but valid $_r$ is chosen along with the same spectral response, a new set of possible layer heights will be generated. This is verified with the full-wave simulator (using the trained forward model), to roughly show the accuracy of each proposed design.
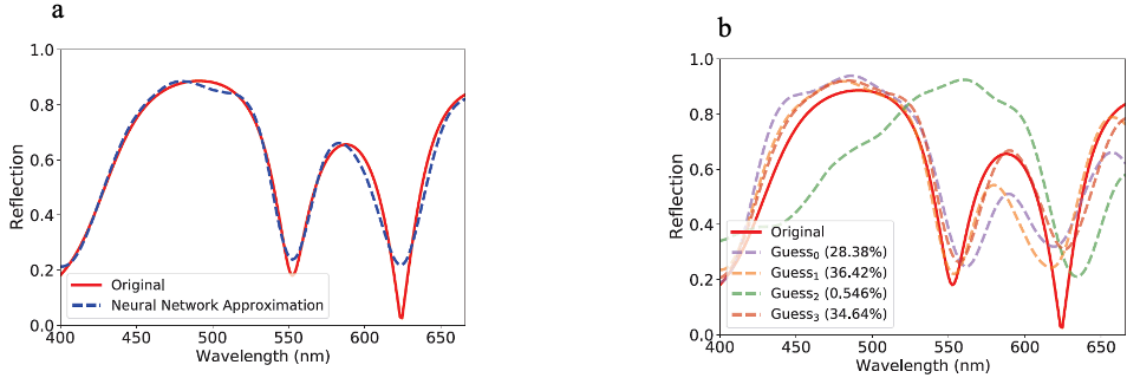
Figure 14 (a) A randomly selected optical response from the test set to try inverse design is simulated with the original design parameters. (b) Displays the simulated responses for MDN suggested designs.

3.5 Conclusion

In the current chapter, I demonstrated a series of DL-based approaches for designing EM nanostructures with a wide range of design possibilities. We showed that by reducing the dimensionality of the response and design spaces using autoencoder and pseudo-encoder, we could convert the initial many to one problem into a one-to-one (or close to one-to-one) problem plus a simple one-to-many problem that can be solved using brute-force analytical formulas. The resulting approach considerably reduces the computational complexity of both the forward problems and the inverse problems. In addition, it also allows for the inclusion of the design restriction (e.g., fabrication limitations) without adding computation complexities.

We demonstrated here a reliable and computationally superior AI approach based on DR for analysis and inverse design of photonic nanostructures. The pseudo-encoder-

based approach has 2-3 orders of magnitude reduction in the required computation for the inverse design of a typical photonic nanostructure without imposing much error compared to using an FNN. It also applies to non-unique problems with no significant difference. By breaking the sizeable non-unique inverse design problem into a sizeable one-to-one problem and a small non-unique problem, our pseudo-encoder-based approach can further facilitate the inverse design of photonic nanostructures, primarily through employing more rigorous optimization techniques for the last stage (from the RDS to the DS). In contrast, such rigorous methods cannot usually be employed for the original non-unique problem due to the excessive computation requirements.

In this chapter, we leverage mixture density networks to choose materials properties and geometric design parameters during the inverse design of nanophotonic structures. We see this strategy as a way to gain intuition about the design problem and give an engineer a pathway to finding suitable designs for desired optical responses. We believe this method can be applied to inverse design problems in general because the tools for searching design spaces are still primitive, and the search spaces are large and obscure. When studying many problems in optics and other engineering disciplines, there is a lack of intuition about choices such as material type and geometry descriptions, while MDNs provide the missing guidance.

CHAPTER 4.   DESIGN FEASIBILITY IN NANOPHOTONICS

This chapter present a distinctive approach for knowledge discovery by bounding the forming the smallest convex/non-convex set to discover hidden optical phenomena while analyzing the feasibility of having a desired optical response from a specific class of nanostructures. The invented techniques reduce the dimensionality of the discovered patterns in the design space and response space while finding the governing geometry of such patterns in lower-dimensional space in which the Euclidean distance can be a good measure for the similarity of different patterns.

Here, I leverage the intelligence aspect of AI for knowledge discovery in nanophotonics. In the next part, I present a new approach based on geometric learning for studying the feasibility of optical responses. This section employs convex-hull formation [51], manifold learning [52-54], and a one-class support vector machine [55] (SVM) to analyze the optical responses underlying behavior.

4.1   Feasibility of the Nanophotonic Structures

Design of photonic devices in the nanoscale regime outperforming the bulky optical components has been a long-lasting challenge in state-of-the-art applications. Accordingly, devising a comprehensive model to understand and explain the fundamental physics of light-matter interaction in these nanostructures is a substantial step toward the realization of novel photonic devices. To this end, existing modeling methods can be categorized into two main groups: single- and multi- objective approaches. Single-objective approaches either rely on exhaustive design parameter sweeps using brute-force EM-solver or evolve

from an initial guess to a final result. Although the former requires extensive computation, the latter highly depends on the initial guess and in most cases converges to a local optimum. Parametrized adjoint optimization can be used to design high-performance nanostructures; however, they are computationally expensive. All of these single objective approaches are computationally demanding and fail when the input-output relation is complex, or the number of the desired features for a nanostructures grows. In contrast, multi-objective methods deal with formation of a model to optimize a certain class of problems. Although these methods are more computationally efficient, obtaining an optimal solution is not guaranteed.

DL-based design approaches, combined with limited exhaustive searches, have proven to be a potent solver of multi-objective optimization problems by learning the input-output relation. Dimensionality reduction approaches show have been shown the effectiveness of reducing the dimensionality of the problem and convert the inverse design problem into a more manageable version of it. More importantly, such novel techniques can provide considerable valuable insight about the dynamics of the light-matter interaction in nanostructures with the hope of uncovering new physical phenomena that can be used to form a completely new types of devices. The change in focus of using DL techniques from "optimization" to "knowledge discovery" can open a new research area with potentially transformative results in the entire field of nanophotonics. Examples of these "knowledge discovery" paradigms include assessing the feasibility of a desired response using a given structure as well as the range of the possible responses a given design can provide. Knowing the feasibility of a desired response offered by a photonic nanostructure is very helpful prior to any design or optimization effort in avoiding suboptimal designs or

convergence issues. It also guides us to modify the initial structure to achieve the desired response.

In this chapter, we present a series of geometric learning- based approaches [47-49] by forming the smallest convex-set to discover hidden optical phenomena while analyzing the feasibility of having a desired optical response from a certain class of EM nanostructures. The developed approach in this chapter is based on reducing the dimensionality of the response space of a given EM nanostructure and funding the convex-hull that contains achievable responses. The technique uses the numerical simulation of the response of the system for a series of similar simulations for validation of the technique. After initial training and validation, the algorithm finds the optimal bounded subset, which contains all feasible responses.

The optimal region that contains the feasible responses might not be convex in many cases, and it is better to find a tighter bound for the feasible region. For this purpose, we use the one-class support vector machine (SVM) algorithm to find the nonconvex geometry. One-class SVM also provides information about the level of feasibility of a response and grants the possibility of trading the acceptable error to get the closest feasible response to an unfeasible one (desired).

4.2 Convex-hull Analysis

4.2.1 Convexity and Convex-hull Formation

The convex-hull of a set of points is the smallest convex set that encompass all the points (see Fig 15). Considering $x_1, x_2, \ldots, x_k \in X$, the convex combinations of these points

is defined as θ_1x_{1+} θ_2x_{2+} $\ldots+$ θ_kx_k where $\theta_i \geq 0$ and θ_{1+} θ_{2+} $\ldots+$ $\theta_k =1$. A set is convex if and only if it contains all the convex combination of its points. The convex-hull of the set of points, X, is denoted as *Conv* X and defined as:

$$Conv\ X = \{\theta_1x_{1+}\ \theta_2x_{2+}\ \ldots+\ \theta_kx_k \mid x_i \in X,\ \theta_i \geq 0,\ i= 1,\ 2,\ \ldots,\ k,\ \theta_{1+}\ \theta_{2+}\ \ldots+\ \theta_k =1\} \quad (5)$$

The convex-hull operator on a set of points: is 1) extensive (i.e. the convex-hull of all sets in X is a superset of X), 2) non-decreasing (i.e., convex-hull of a subset X, is a subset of the convex-hull of X), and 3) idempotent (i.e., the convex-hull of the convex-hull of X is same as the convex-hull of X). The convex-hull of any set of points is also unique and closed set.
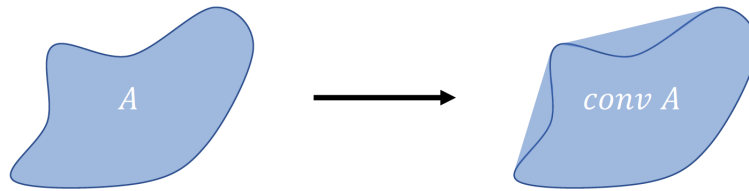
Figure 15 Set A shows a non-convex set of points. The convex-hull (i.e., *conv* A) of this set is the smallest convex set that contains all the points in set A.

There are different algorithms presented in geometrical computation to form the convex-hull of a given set of points. One of the most effective and well-known algorithms is Quick-hull. This algorithm finds the convex-hull of a set of points in d dimensional space using an effective method both in memory and computation. Given a set of n data points with r processed points, the algorithm is O(n log r) for d≤3 and is O(n f_r/r) for d>3 (f_r is the maximum number of facets for r vertices). The extreme points of a convex-hull are

referred as the vertices of the boundary of the convex-hull. The computation complexity of the algorithm depends on the number of facets and vertices of the convex-hull. Therefore, for sets with fewer extreme points it takes less time for the algorithm to find the solution. A d-dimensional convex-hull can be shown using its vertices and the (d-1)-dimensional facets. The ridges of the convex-hull can be shown using its vertices and (d-2)-dimensional facets which are the intersection of the vertices in two neighbouring facets. Quickhull forms the convex-hull using an incremental method based on Grunbaum's Beneath-Beyond theorem (See Figure 16) as the following:

Grunbaum's Beneath-Beyond Theorem: Consider H as the convex-hull of a set of points in R^d and a point p outside the convex-hull in R^d-H. F is a facet of *Conv* $(H \cup p)$ if and only if:

1) F is a facet of H and p is below F, or

2) F is not a facet of H, and its vertices are p and the vertices of a ridge of H that has one incident facet below p and one above p.

Figure 16 Quickhull algorithm adds the farthest point in the outside set to the convex-hull at each iteration. The outside sets, the facets, ridges, and vertices will be updated in each step. This process continues until there is no outside point.

The Quickhull algorithm starts with a set of points (i.e., a random subset of all training datapoints) and forms the initial convex-hull. All the points that lie outside of the initial convex-hull are considered as the outside set. The furthest point from the outside set is found at each iteration and based on Grunbaum's Beneath-Beyond Theorem, the facets, ridges, and vertices will be updated (see Fig. 16). This process will continue until convergence. The resulting convex-hull consists of all datapoints.

After forming the convex-hull for a set X in the latent space, we need to find out whether a given point p lies inside the convex-hull or not. We first consider a random point *a* outside of the convex-hull. We then connect x and a with a line segment *xa* and find the number of its intersection with every of the convex-hull. If the number of intersections is odd, the point lies inside the convex-hull. Otherwise, if the number of the intersection is even or zero, this point is outside the convex-hull (see Fig 17).
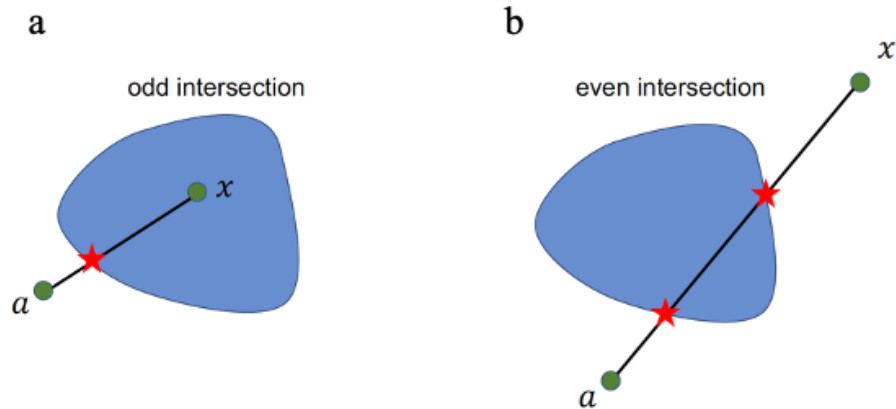
Figure 17 The schematic of Inhull function for finding points inside and outside the convex-hull. To check if a sample point x is inside or outside the convex-hull, the

algorithm considers with the convex-hull. If the number of intersections is odd, the point x is inside (part a) and if it is even (part b), x is outside the convex-hull.

4.2.2   *Convex-hull Analysis for Bounding Feasible Responses*

Figure 18 shows the schematic of our invented technique [47] for forming the convex-hull for the feasible responses of a given nanostructure. In the first step, a full-wave EM simulation software provides an initial batch of randomly generated patterns. Each pattern is calculated using a given set of randomly selected design parameters. Then we reduce the dimensionality of the response space by training an autoencoder utilizing a subset of the available training data and the desired reconstruction error. Next, we use the Quick-hull algorithm to form a convex-hull to bind the response space patterns. Then we validate the convex-hull utilizing a batch of validation data. As all of the validation data originate from a feasible structure, the optimum convex-hull should bound all the validation data. We put a threshold for the validation success rate. If convex-hull does not pass the validation step, the validation batch will be added to the initial training batch to expand the training dataset for retraining the algorithm. After convergence, the convex geometry is tested using the unseen test dataset (that includes both feasible and unfeasible responses) to find its performance defined by the error rate.
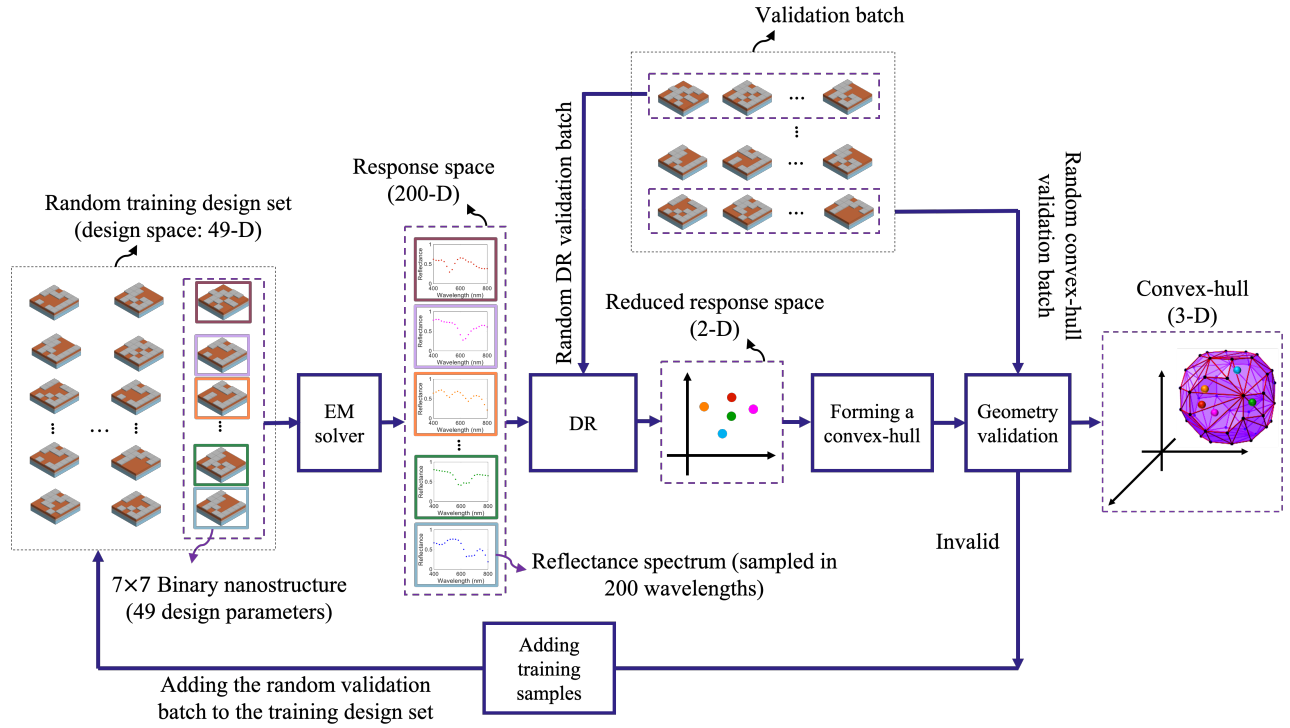
Figure 18 Training algorithm for finding the convex-hull of the patterns in the latent response space. The 2-D and 3-D representations are just examples for facilitating graphical understanding [47].

To demonstrate our technique's potential, I apply it to investigate possible optical reflection responses from the binary nanostructure in Fig. 6c with different pixilation levels (i.e., 7×7 and 14×14). The design patterns in each case are achieved by a random selection of the binary inclusions. The calculated reflection spectra are sampled uniformly over the 400-800 nm range wavelength range with 2nm resolution to form a vector with the dimensionality of 200 as the response pattern. Due to the algorithm's iterative nature in Fig. 18, the minimum number of training data depends on the number of iterations for convergence. Besides, we use 500 simulated response patterns for testing the algorithms after convergence. Based on several simulations to understand the selected structures'

requirements, I chose 8000 as the training/validation dataset size. Knowing that achieving an ideal Fano line shape is not possible with these structures (due to the tremendous ohmic loss of metals in the visible range), in a collaboration with our groupmate, we also formed 80 perfect Fano line shapes over the 400 – 800 nm spectral range unfeasible responses to test the algorithms.

After obtaining the training dataset, the first step of the implementation is the DR of the response space by training an autoencoder. We select the latent response space's dimensionality as 6 to meet the threshold of 0.001 MSE, translating to less than 5% point-to-point error. It is important to note that this initial training step aims to find the autoencoder's optimum dimensionality. We use an untrained autoencoder with the optimum dimensionality and train the entire algorithm. To find the optimum convex-hull in the resulting response space, we start with an initial batch of data with 5000 ground-truth patterns in the algorithm in Fig. 18 to train the cascaded autoencoder forming the convex-hull in the 6D latent space. We use 200 validation data (without replacement) for autoencoder and 200 for the convex-hull. We select 5% point-to-point error for the autoencoder validation threshold and 95% for in-point percentage (i.e., rate of the ground-truth patterns lies inside the boundary), respectively. The algorithm converged after 14 iterations. As a result, we used 11000 data to reach convergence. Figure 19a shows that using 6 as the dimensionality of the latent response space results in MSE of 0.001, which can be translated to less than 5% point-to-point error.
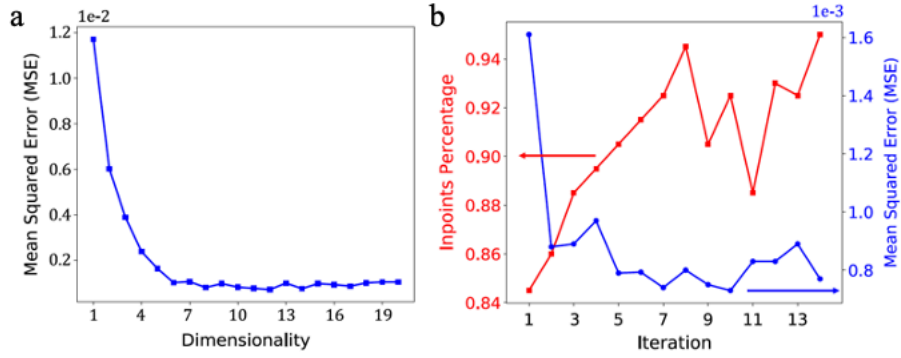
Figure 19 (a) Reconstruction MSE for autoencoder trained on the responses of the 14×14 binary structure in Fig. 6c for different dimensionalities of the latent response space. Using the result, 6 is selected as the desired dimensionality of the latent response space. Response can be reconstructed after reducing dimensionality from 200 to 6 by accepting less than 5% error. (b) Auto-encoder training error and in-point percentage for the algorithm in Fig. 18 after different iterations of the algorithm. The algorithm converged after 14 iterations.

Table 2 In-point percentage of each class of test parameters lines in 2-D, 3-D, and 6-D convex-hull as well as one-class SVM highest confidence region

Algorithm class	Binary 14×14 %	Binary 7×7 %	Fano line shapes %
Convex 2-D	99.2	100	35
Convex 3-D	98.6	99.8	10
Convex 6-D	91.8	96	0
One-class SVM 2-D	90.2	90.6	0
One-class SVM 3-D	91.4	89.4	0
One-class SVM 6-D	88.2	84.4	0

4.3 Finding the Non-convex Boundary of The Feasible Responses

4.3.1 One-class Support Vector Machine

Assume that the training data are x_1, x_2, ..., $x_k \in X$ where N is the numberof datapoints. Considering the mapping $\varphi(x)$ from the feature space, X, to a Dot Product space F, the kernel function is defined as:

$$k(x_i, x_j) = <\varphi(x_i), \varphi(x_j)> \tag{6}$$

There are different choices for the kernel function like Gaussian and polynomial kernel. In this chapter we use Gaussian kernel.

$$k(x, x) = e^{-\frac{\|x-y\|_2^2}{\gamma}} \tag{7}$$

One-class SVM can be formulated as an optimization problem which finds a hyperplane to separate datapoints in X from the origin in F and has the maximum distance from the origin. The problem is formulated as a quadratic program:

$$\min_{w \in F, \xi \in \mathbb{R}^N, \rho \in \mathbb{R}} \frac{1}{2}\|w\|_2^2 + \frac{1}{\nu N}\sum_{i=1}^{N}\xi_i - \rho \tag{8}$$

$$s.t. <W, \varphi(x_i)> \geq \rho - \xi_i \ \forall i \in \{1, 2, .., N\}$$

By solving the optimization problem through quadratic programming, the decision function becomes

$$f(x) = \sum_i \alpha_i k(x_i, x) - \rho \tag{9}$$

Here, ρ can be recovered using the dual variables (i.e., α_i). The datapoints x_i with their corresponding optimized nonzero α_i is called support vector. These datapoints are close to the boundary and enforce the complexity of the boundary.

4.3.2   *One-class Support Vector Machine for Probabilistic Feasibility Analysis*

Although the convex-hull algorithm can find a convex geometry for possible responses, it has some limitations. If the optimum feasible region is not convex, inevitably, some unfeasible areas of the latent response space will be included in the convex-hull to reach a convex region. This limits the efficiency of the algorithm for such structures due to false-positive errors. Moreover, the algorithm acts as a binary classifier and classifies responses into two classes: feasible (achievable) and unfeasible (unachievable). It is desirable to know how far an unfeasible response is from viable responses in most practical cases. It is also helpful to see whether it is possible to push an unfeasible response toward the feasible region by accepting some error. Unfortunately, the Euclidean distance of a given point in the latent response space from the convex-hull boundaries is not a good measure for the corresponding response's feasibility. To address this limitation, I use one-class SVM. Figure 21 shows the schematic of the one-class SVM technique. As Fig. 18, a similar process is used for training the one-class SVM to find the non-convex geometry of feasible response patterns in the latent space.
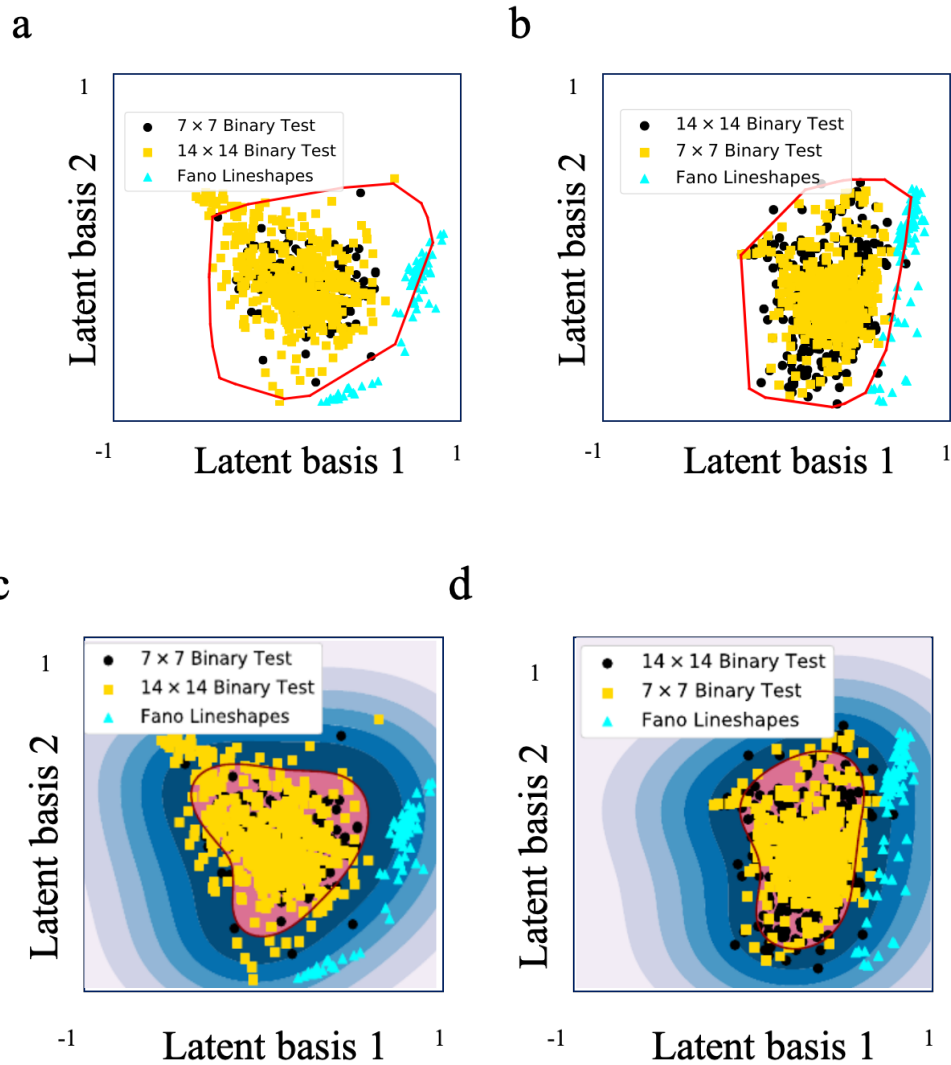
Figure 20 Representation of the convex-hulls for (a) 7× 7 binary structure in Fig 6c and (b) 14×14 binary structure. The possible responses for the 7× 7 and 14×14 binary designs and the infeasible ideal Fano line shapes are shown. Representation of the non-convex boundary and the confidence intervals for (c) 7× 7 binary structure and (d) 14×14 binary structure.
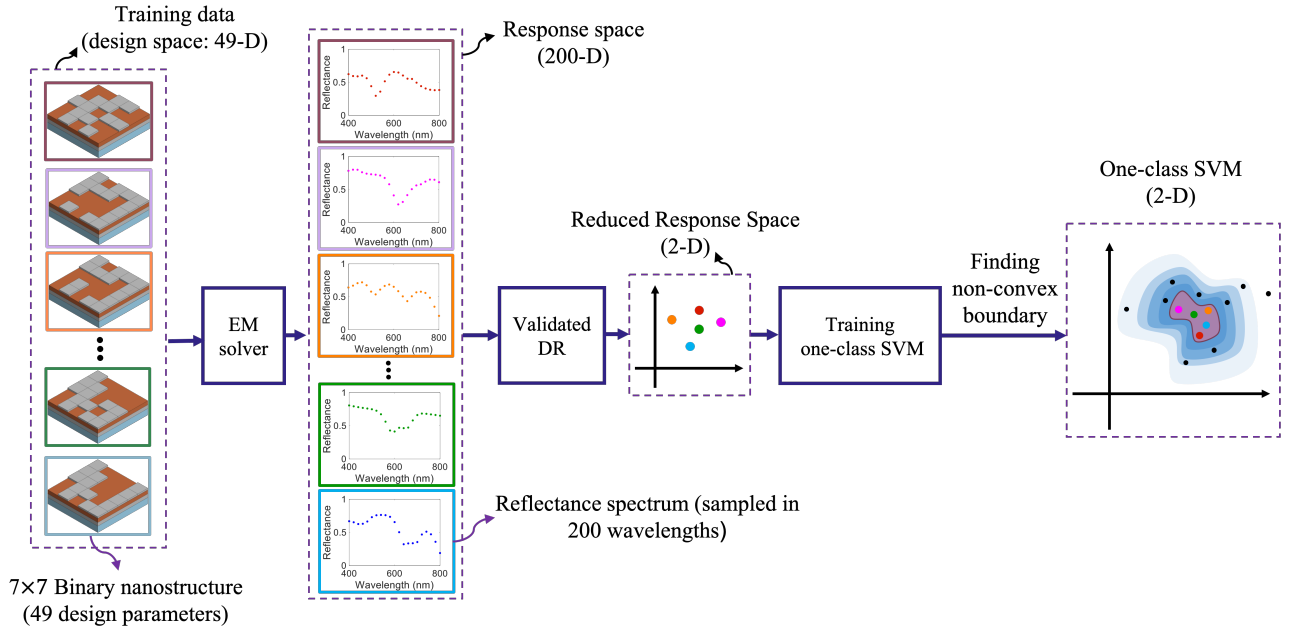
Figure 21 Using one-class SVM over patterns in the latent response space to investigate the level of feasibility of the desired response. The dimensionality of the latent response space is found by training autoencoder [47].

I apply the developed technique to the same problem that we had in the previous section to add the luxury of forming a tighter boundary for the possible responses. We use the same training data to train a one-class SVM for the structure in Fig. 6c using 6-D, 3-D, and 2-D latent reactions. Although one-class SVM provides valuable information about each desired response's relative feasibility, finding the optimum hyperparameters.

Despite training with a nonaggressive success rate of 95%, the convex-hull algorithm is capable of identifying all unfeasible responses as well as a large portion of feasible responses. For example, it is not trivial to compare the robustness of the resulting designs for achieving two responses as there is not a simple one-to-one relation between the Euclidean distance to the convex-hull boundary and the feasibility of the response. To
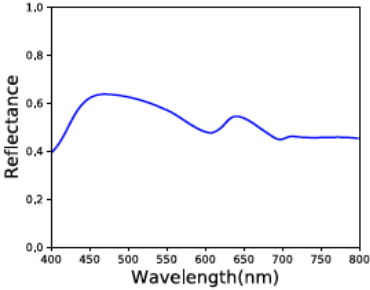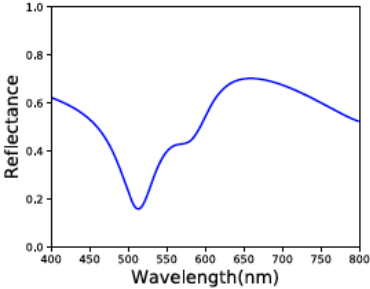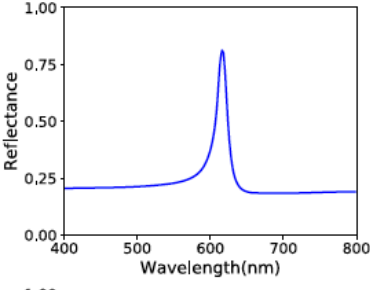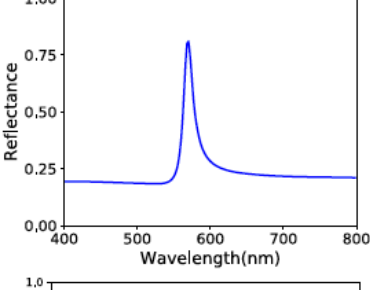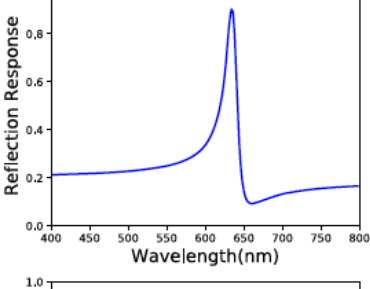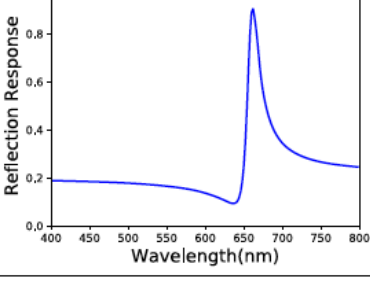
add this feature, I use the same training/validation data to train a one-class SVM to find the nonconvex geometry of the feasible responses for the structure in Fig 6(c) using 6D, 3D, and 2D latent RSs. Although one-class SVM provides valuable information about the relative feasibility of each desired response, finding the optimum hyperparameters (i.e., ν and γ) for one-class SVM is challenging. Here we use 500 validation patterns to cross validate the hyperparameters the hyperparameters and find $\nu=0.4$ and $\gamma=4$ as the optimum parameters.

Table 2 shows the result of testing the 6-D, 3-D, and 2-D one-class SVM algorithms with the same data used for testing the convex-hull algorithm. Lower success rates in identifying the possible responses while perfect performance in identifying unfeasible responses are attributed to the one-class SVM tighter geometry. This is also seen from the graphical representation of one-class SVM in the 2-D latent space. Note also the absolute values of the success rates in Table 2 for one-class SVM depend on the highest confidence region's definition. Reducing the level of confidence results in an extension of its corresponding geometry and thus a smaller error. In addition to the innermost geometry (highest confidence region) shown by red curves in Fig. 20c and 20d, several boundaries are identified with different colors. Each added region corresponds to a different level of the unfeasibility of a response in this one-class SVM is the minimum Euclidean distance of that response from the boundaries of the highest confidence region. A quantitative measure for the level of feasibility of a response is the minimum Euclidean distance of the response from the boundaries of the highest confidence region. The calculated distance in the 6-D one-class SVM for a series of responses of the structures is shown in Table 3. The average distance for each class of responses in Table 3 is calculated over the entire set of

those responses in the test dataset. In addition, for each class, a representative sample response and its actual distance from the geometry are shown. A negative/positive distance shows that the point lies outside/inside the highest confidence region; the absolute value of the distance shows the relative unfeasibility of a response. Table 3 clearly shows that a smoother response (the first row of Table 3) has a better feasibility than a sharper one (the second row of Table 3). It also confirms the unfeasibility of the ideal Fano and Lorentzian responses with Fano responses being farther from the feasibility region.

It is important to note that the goal this initial training step is to find the optimum dimensionality of the autoencoder. For optimal training of either algorithm (See Fig. 18 and Fig. 21), we use an untrained autoencoder with the optimum dimensionality and train the entire algorithm (composed of the autoencoder follows by the Quickhull to form the convex geometry). To find the optimum convex-hull in the resulting latent response space, we start with an initial batch of data with 5000 ground-truth patterns to train the cascaded autoencoder and forming the convex-hull. At each iteration we use 200 validation data (without replacement) for autoencoder validation threshold and 95% for in-point percentage (i.e., percentage of the ground-truth patterns lies inside the boundary), respectively. The algorithm converged after 14 iterations. As the result, 11000 training instances has been used to reach the convergence.

Table 3 Average distance of different classes of test data (14by14 and 7by7 responses as well as Fano and Lorenzian lineshape resonances) from the highest confident region border for one-class SVM. Distances for random samples represented in the most right column

	Average distance	Sample distance	Sample plot
Binary 14 × 14	60.89	128.44	
Binary 7 × 7	56.08	15.36	
Lorentz shape 1	−74.57	−62.53	
Lorentz shape 2	−72.70	−46.75	
Fano shape 1	−85.02	−60.71	
Fano shape 2	−80.39	−117.51	

4.3.3   Analyzing Infeasibility of Optical Responses for a Binary Nanostructures

As an experiment we simulate 21 random cylindrical nanostructures and obtain the corresponding response (see Fig. 22b). Then, I formed the nonconvex boundary of the feasible responses for the binary nanostructure in Fig. 6c. Figure 22 represents the location of those 20 responses on the 2-D latent space. As we can see the responses which has resonances in lower wavelengths and sharper resonances (e.g., 2, 10, and 12) are located in the outer region of the nonconvex boundary (represented by moving toward the lighter blue region). Such intuition about the capability of the structures in providing an specific response could help us in select a better type of structures (e.g., material, geometry, and size) and as the results push the highest possible accuracy for any design approaches.
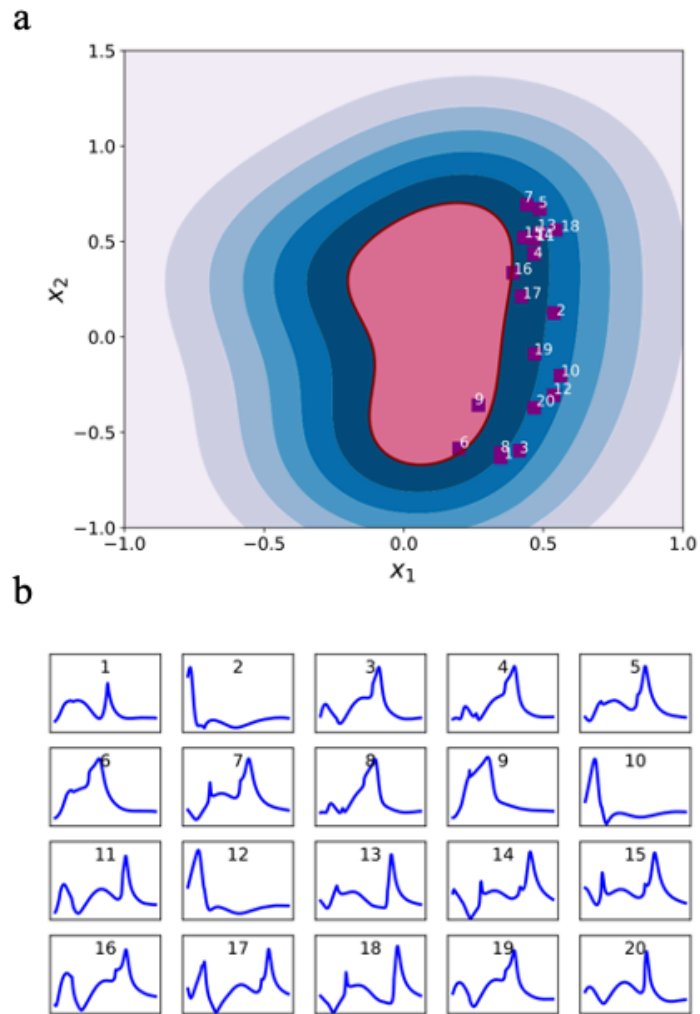
Figure 22 (a) The trained one-class SVM for 14×14 structure in Fig. 3c. (b) Representation of the 20 random reflection responses achieved from another nanostructure. The corresponding number for each response is shown in the one-class SVM in (a).

The results in Fig. 20 and Fig. 22 show the power of geometric learning algorithms in assessing the feasibility of a desired response given a specific nanostructure design. They also show the advantage of one-class SVMs in providing a more quantitative measure for

the level of feasibility of the desired response. The advantage comes from the boundaries of the one-class SVM, the geometric distance of a point in the latent RS from the boundaries of the one-class SVM is a good measure for the feasibility of the response, whereas in convex-hulls, this relation does not hold necessarily. This advantage comes at the expense of more sophisticated training as the optimum hyperparameters ν and γ in SVM are not usually trivial to find. This advantage comes at the expense of more sophisticated training as the optimum hyper parameters ν and γ. Nevertheless, convex-hulls are helpful in providing the quick evaluation of the feasible response feasibility. The training process can also be simplified if more error is accepted. Note also that finding the exact geometry of the convex-hull and one-class SVM may not be important in design and optimization problems as the points on the boundaries correspond to less reliable responses that are prone to environmental changes or fabrication errors. We prefer the desired response to be in the middle of the one-class SVM.

In addition to the boundaries of convex-hull and one-class SVM in the latent RS, the area that is covered in that space by these shapes has important practical implications. The larger the area, the more capable the structure is in forming varieties of output responses. Figure 20 shows convex-hull and one-class SVM in the 2D latent RS of the binary nanostructure in Fig. 6c formed by 7×7 and 14×14 array of nanostructures. For comparison, the responses used for the testing of the 14×14 structure also provided. It is clear that the convex-hull and non-convex bound for the 7×7 nanostructure cover a smaller percentage of the 2D latent RS than those of the 14×14 structure. This conclusion must be taken with the caveat that the latent RSs for the two structures are not necessarily the same. Note that a wider range of responses may or may not be desirable for the design. For

61

reconfigurable structures, a wider response range usually is considered as unnecessary complexity of the selected structure. Figure 20 clearly shows that while technically none of the responses of the 7×7 structure was used in training the convex-hull and one-class SVM of the 14×14 nanostructure, all these responses fall inside the convex-hull and one-class SVM as any 7×7 structure can be formed using the 14×14 structure. Figure 19a and (c) also show that some of the responses achieved by 14×14 structure cannot be achieved using the 7×7 structure, whereas some of them can. This is an important observation as it confirms that using 14×14 nanostructure for some responses might be unnecessary; the same response can be achieved by a much simpler structure with less fabrication challenges and more robustness against fabrication imperfection. I believe this observation is an important potential application of the convex-hull and one-class SVM in finding the most robust and least complex structures when the desired response falls in the middle of the one-class SVM (i.e., has maximum distance from the boundaries) results in more tolerance against environmental changes and fabrication imperfection.

The DR algorithm implemented by the autoencoder is an important step in reducing the required computational resources for the convex-hull and one-class SVM. For any particular problem, the optimum dimension of the latent RS depends on the selection of the design and the redundancy of the response (i.e., level of non-uniqueness). Thus, finding the optimum size of the latent RS is the initial step in implementing the developed techniques. Once the size of the latent RS is selected, the required computation for the calculation of the convex-hull and one-class SVM is primarily for the training algorithm. In this section we mainly used the brute-force approach in starting with a training dataset and expanding it until the convex-hull pass the validation test. Further rigorous approaches

must be developed to minimize the computation required for training. One can also take advantage of the trade-off between the accuracy and the computational cost to optimize the training approach as explained earlier. Although the focus of this chapter was first demonstration of feasibility study for a given response, the technique can be adopted for obtaining far more detailed information about the physics of nanostructures.

The invented technique can also facilitate the design of nanostructures using conventional inverse problem-solving approaches such as genetic algorithms that focus on finding the design parameters of a selected structure without carefully studying the feasibility of achieving the desired response using the selected design. These techniques can use our approach as an initial feasibility study step to ensure the selected structure for the optimization procedure to avoid unnecessary complex designs and reduce the fabrication challenges. The invented technique can be optimally combined with any optimization technique to provide a guideline about the feasibility of a desired response and reduce the computation complexity of the inverse design problem.

4.4   Conclusion

In this chapter, I presented a new approach to utilizing AI to study nanophotonic structures' feasibility by training two well-known algorithms (convex-hull and one-class SVM) [47-49]. I showed that by combining the convex-hull (or one-class SVM) with DR by an autoencoder, we could find the range of possible responses and the degree of the feasibility of the desired response from any given class of EM nanostructure in its latent RS. By applying these techniques to a series of nanostructures, I showed the unique capabilities of one-class SVM and convex-hull in providing valuable insight into any EM

nanostructure's capabilities in providing different types of responses. While this is the first demonstration of an AI-based approach for such knowledge discovery, the presented techniques show great potentials in facilitating the understanding of the underlying physics of EM nanostructures and forming a more systematic approach in designing such nanostructures.

CHAPTER 5.   ARTIFICIAL INTELLIGENCE FOR KNOWLEDGE DISCOVERY IN NANOPHOTONICS

In this chapter, I presented a series of new methods for knowledge discovery in nanophotonics through latent learning. I showed that combination of the DR, manifold learning and convex-hull formation can provide priceless information about the level of feasibility for achieving a desired response given we want to use a certain class of nanostructure. By applying these techniques to a series of nanostructures, I showed the unique capability of the technique in providing valuable insight about the capabilities of manifold learning in providing different types of responses. Although this the first demonstration of an AI-based approach for such knowledge discovery, the presented techniques show great potentials in facilitating the understanding of the underlying physics of EM nanostructures as well as forming a more systematic approach in designing such nanostructures.

5.1   Shallow Pseudo-encoders for Mining the Roles of Design Parameters

Our approach's main advantage is the possibility of investigating the underlying physics of the device operation and obtaining intuitive information about the role of different design parameters on its response [37-39]. To show this capability, we use our approach with a pseudo-encoder to model the nanostructure in Fig. 6d. Figure 23a shows the resulting pseudo-encoder with the reduced design space dimension being four with green and red arrows representing positive and negative weights, respectively. Note that the DR of the design space is performed with only one encoder layer. The strength of the

connections is shown in Fig. 23a by the color opacity. As shown in Fig. 23b, the crystallization levels l_{c1}, l_{c2}, l_{c3} can only change one of the reduced response features as they mainly connect to one node (the purple node) in the bottleneck layer. As a result, as long as the total input to that purple node is fixed, the response will stay the same regardless of how the values of lc_1, l_{c2}, l_{c3} can change. This conclusion is reached by assuming a small error in training the pseudo-encoder and neglecting the small weights (or arrows in Fig. 23a) connecting l_{c1}, l_{c2}, l_{c3} to the nodes bottleneck layer. To test this conclusion, we vary l_{c1}, l_{c2}, l_{c3} while keeping their weighted sum (according to the trained pseudo-encoder) and all other seven design parameters for the nanostructure in Fig. 6d, and we calculate the response of the nanostructure using brute-force COMSOL simulation (no pseudo-encoder intervention). The results for two different weighted sums are shown in Fig. 23b. The figure confirms our observation from the pseudo-encoder that l_{c1}, l_{c2}, l_{c3} effectively act as a single design parameter. This suggests that the parameter h can be used to obtain different classes of responses while weighted sum of l_{c1}, l_{c2}, l_{c3} can be used to finely tune a given class of response. The details of the design parameters for each case are shown in Table 4.

Table 4 The design parameters and the resulting MSE for the optimal design and three good designs for the structure in Fig. 6d to achieve maximum absorption in the 1500-1700nm wavelength region. h, w_i , and pi {i=1,2,3} are in nm.

Design	h	l_{c1}	l_{c2}	l_{c3}	P1	P2	P3	W1	W2	W3	MSE
D_1	190	0.5	0.6	0.7	650	650	550	350	500	200	0.0147
D_2	190	0	0.2	0.8	650	650	350	450	250	250	0.0149
D_3	190	0.5	0.1	0.7	650	450	450	200	350	300	0.0152
D_4	190	0.3	0.6	0.8	650	550	550	250	300	450	0.0172

Figure 23 (a) The pseudo-encoder architecture trained for the problem in Fig. 3d, which relates the design space to the reduced design space. Green and red colors and opacity represent the positive, negative signs and the coupling strength. (b) Red curves correspond to three different l_{c1}, l_{c2}, l_{c3} where their weighted sum for the purple node is the same. Blue: similar three curves but for another weighted sum [36].

While some of the conclusions about the role of design parameters in Fig. 23 obtained by training the pseudo-encoder could also be obtained by the underlying mode properties of the DL-based (e.g., by analyzing the modes of plasmonic resonators), the ability of our approach in providing useful information about the physics of wave-matter interaction in non-trivial structures (e.g., nonlinear and dispersive metamaterials) will be extremely valuable. Indeed, by using this approach to find and understand new phenomena in such non-trivial structures, new ideas for forming new classes of devices can be generated. This is a major advantage of our approach over all existing design approaches, especially those that rely on multiple brute-force simulations of the structure for different design parameters.

Note that the MSE (about 10%) in relating the design and response spaces using the mono-layer pseudo-encoder in Fig. 23b is larger than that a more complex pseudo-encoder. Nevertheless, the intuitive understanding of the roles of the design parameters achieved with the simple pseudo-encoder is completely valid. While the mono-layer structure provides simple and helpful information about the role of design parameters, more sophisticated relation (and physics) can be learned by using a pseudo-encoder with more layers and studying the NN weights in the different layers. It is also evident that the algorithms selected for understanding the physics of the wave-matter interaction are in general different from those used for design and optimization of the structure to achieve a desired response. In the latter the minimization of the MSE in the input-output relation is critical while in the former it is the secondary importance.

5.2 Manifold Learning: An Ultimate Approach for Response Analysis in Nanophotonic Structures

To form a comprehensive playground for optical response analysis, we developed a new toolkit [56-58] based on manifold learning to extract underlying behaviors of responses for different nanostructures classes. The approach also provides valuable information for designing nanostructures by discovering the governing physics of light-matter interaction in the nanoscale regime. Among other manifold learning techniques (e.g., Isomap, t-distributed stochastic neighbour embedding, LLE), multidimensional scaling, and unified manifold approximation and prediction), I believe LLE is the most suitable approach to our application due to its unique features in preserving local information in the low-dimensional space.

The developed method employs LLE to study the modality of the possible responses for each class of nanostructures. LLE finds the *K* nearest neighbours in the original space y, then calculates the optimum set of weights to reconstruct point y_i from its neighbors while minimizing the cost function *L* calculated as:

$$L(w) = \sum_{i=1}^{N} \left\| y_i - \sum_{j=1}^{K} w_{ij} y_j \right\|^2 \tag{10}$$

To find the minimum value for Equation 10, I solve an N×K linear equation for all training data neighborhoods. The resulting w captures a sufficient amount of geometrical information of the patterns by minimizing the cost function. Next, the LLE algorithm finds the latent patterns (vector z) using the optimum weights (i.e., $\hat{w}$).

$$L(z) = \sum_{i=1}^{N} \left\| z_i - \sum_{j=1}^{K} \hat{w}_{ij} z_j \right\|^2 \tag{11}$$

The optimization problem in Equation 11 can be defined as a root problem of solving partial eigenvalue decomposition.

To show the technique's potential, I apply the algorithm to a set of EM spectral responses achieved from the metasurface structure in Fig. 24a to study the optical reflection spectra's modality [56]. The structure is composed of hydrogen silsesquioxane (HSQ), GST silicon (Si), and silicon dioxide (SiO_2). GST is a type of PCM, which provides the luxury of controlling material properties (e.g., change in refraction index). This tuning can be done via an external stimulus (e.g., heat or voltage).

The structure has six geometrical design parameters: r, p, h_{HSQ}, his, h $_{SiO2}$, and h_{GST}. To generate the training data, we calculate the reflection spectra of 2400 different

geometries selected randomly. For each set of geometrical parameters, in a collaboration with our groupmate, we simulated GST with 11 uniformly distributed crystallization levels. Each of the calculated reflection spectra is uniformly sampled at 1000 wavelengths in the desired wavelength range of 1000-1700 nm, resulting in 1000-dimensional response space. To find the low-dimensional visual representation of the reflection spectra, I apply LLE to 22880 reflection responses while keeping the MSE as the accuracy measure for the algorithm. I use the validation dataset to find K=10 as the nearest neighbors' optimum number to map the training data to the low-dimensional manifold using the validation dataset.

Each sub-manifold represents the range of responses available from the metasurface with one of the 11 GST levels. This technique provides an intuitive visual representation of the nanostructure's detailed reflection spectra with different design properties and GST phases in low-dimensional space. It also enables us to follow the evolution of the metasurface responses upon changes in the GST phase or the nanostructure's geometrical parameters.

As shown in Fig 24b (i) and (ii), each crystallization level owns a specific sub-manifold in the latent space. This indicates the crucial role of material characteristics in providing a wide range of responses. Figure 24b (iii) shows the spectral response's gradual evolution by changing the GST crystallization level.
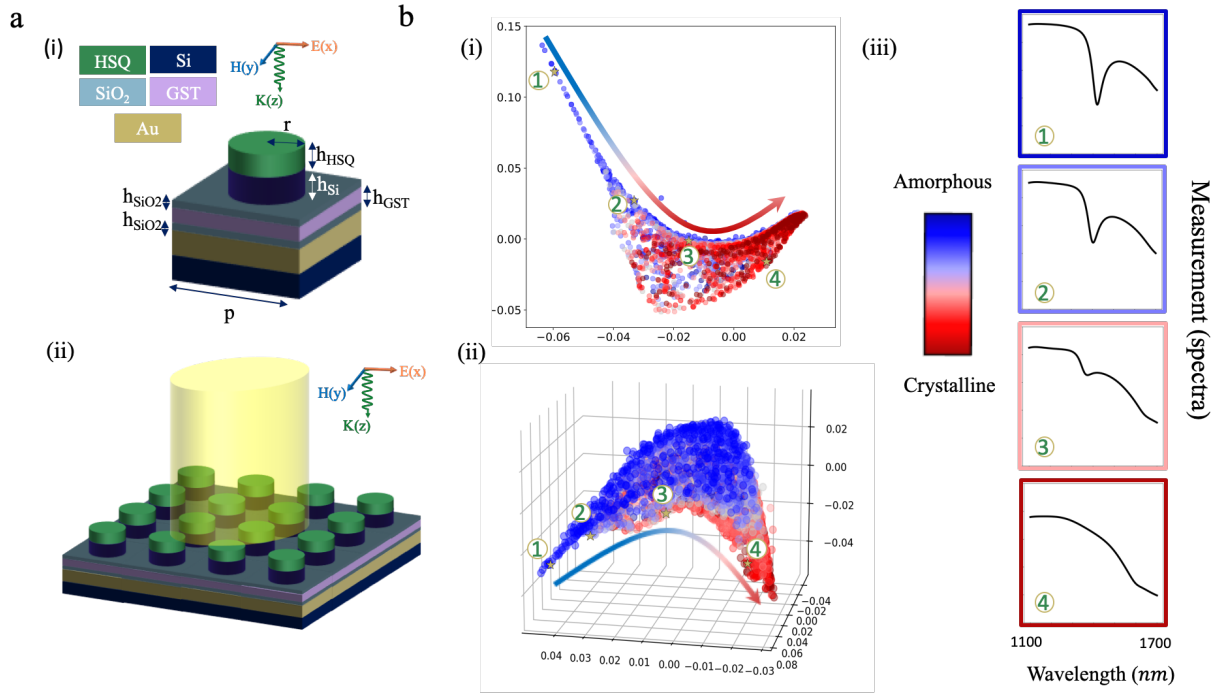
Figure 24 Representation of a multilayer metasurface [56] with (a) a single nanodisk. The pitch of the cell (p), the radius of the nanodisks (r), and thickness of the top and bottom layers (hᵢ) are design parameters, (ii) Exciting an array of nanostructures in part (i) with a plane wave along the z-direction. (b) Applying LLE to the spectral responses of the nanostructure in part a. (i) Two- and (ii) three-dimensional manifold for amorphous and crystalline states, and nine intermediate states. (iii) representation of the modality changes in the reflectance spectra for a single geometrical design and four different crystallization levels.

5.2.1   Analyzing the Role of Material Characteristics in Forming Optical Responses

While the effect of geometry is always a subject of study in inverse design of nanostructures there has been no effort (to the best of our knowledge) to study and design the geometry and material at the same time. In this part we employed manifold learning-

71

based technique to learn and design both geometry and material. To show the capability of the technique I employed the method to design the nanostructure in Figure 24a.

Figure 25 represent the 3-D representation of the response instances for the nanostructure in Fig. 24. It is clearly shown that the responses formed different region based on their material characteristics (i.e., crystallization levels) even in the cases that they have same geometrical features. Such valuable understanding could provide use information about the underlying physics of light-matter interaction while guiding the intelligent design technique to select a better geometry and material as the starting point.

Figure 25 Representation of the 3-D manifold of the responses achieved by structure in Fig. 6b using LLE from different angles. Colors (blue/red) represent the crystallization level of the GST (Amorphous/Crystalline).

Manifold learning approaches can be categorized in two main groups, methods which learn the local features and ones with focusing on preserving the global relations. For different algorithms the low-dimensional manifold is formed differently. In using manifold learning for knowledge discovery in nanophotonics this feature is more leaned toward being an advantage than being a shortcoming as we like to observe different type of clustering and use that as a hint to come up with a conjecture, generalize it by adding more simulation datapoints, and finally turn that to a hypothesis.

In Figures 26 and 27, I applied different manifold learning technique to analyse the optical response that we get from the nanostructure in Fig. 24a for three different crystallization levels. As we can see different methods cluster responses in a different way and this could help the designer analyse the underlying features from different aspects and come up with a more strong understanding/hypothesis about the relation of the material characteristics and the optical response. Here we could clearly see different crystallization levels cover different part of the manifold and by walking on the underlying manifold we can pave different regions that could be translated as having the desired response is just doable in a specific crystallization level.

a PCA

b Kernel PCA

c LLE

d t-SNE

● Amorphous
● Intermediate
● Crystalline

e MDS

f Autoencoder

g Convolutional Autoencoder

h UMAP

74
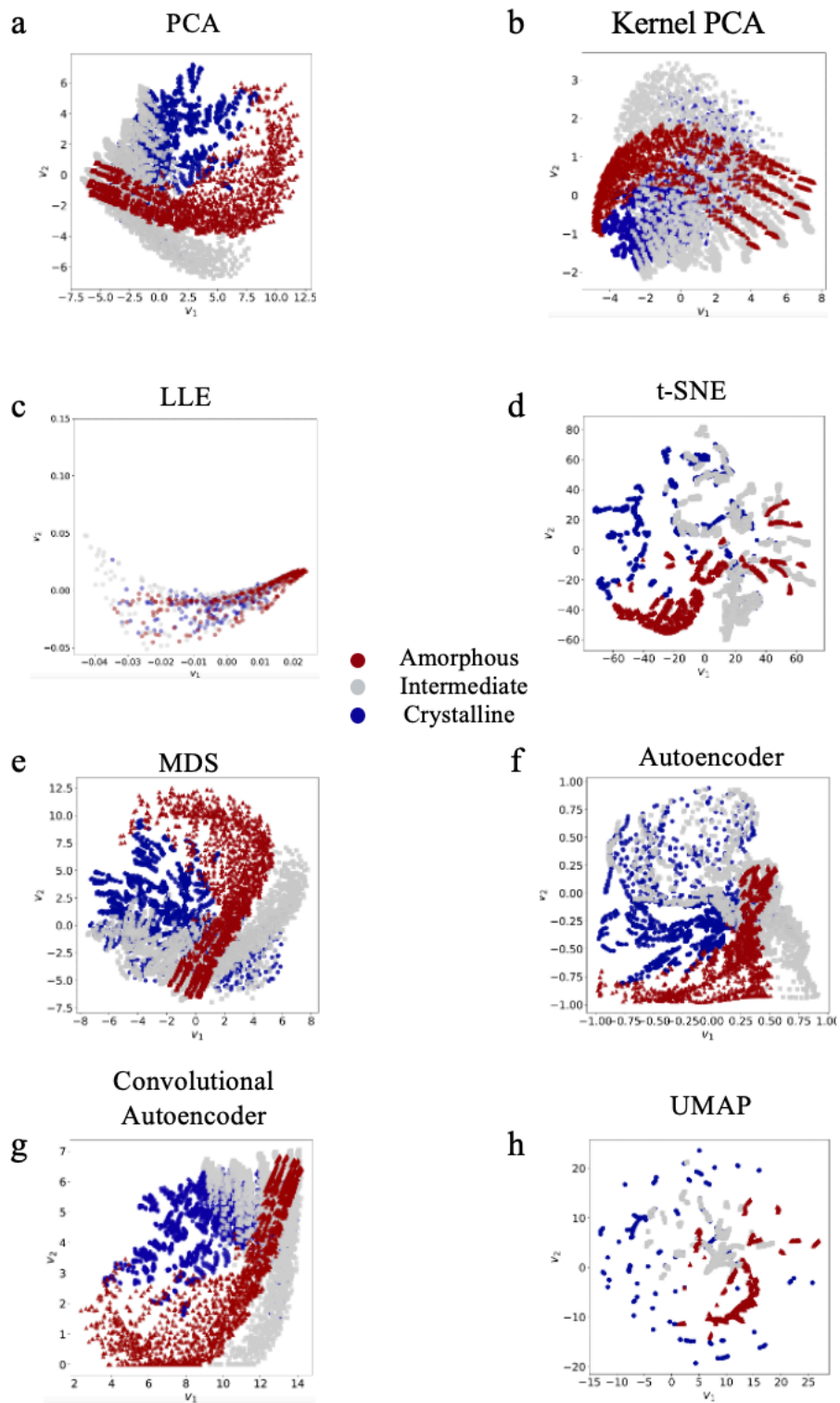
Figure 26 Representation of the 2-D manifold of the responses achieved by structure in Fig. 24a using different manifold learning approaches. Colors (blue/red/gray) represent the crystallization level of the GST (amorphous/crystalline/intermediate stage). (a) PCA, (b) kernel PCA, (c) LLE, (d) t-SNE, (e) MDS, (f) autoencoder, (g) convolutional autoencoder, and (h) UMAP.

PCA

a

Kernel PCA

b

LLE

c

t-SNE

d

● Amorphous
● Intermediate
● Crystalline

MDS

e

Autoencoder

f

Convolutional
Autoencoder

g

UMAP

h

76
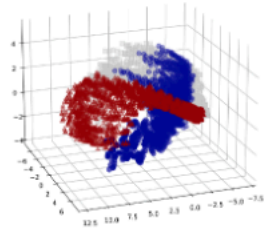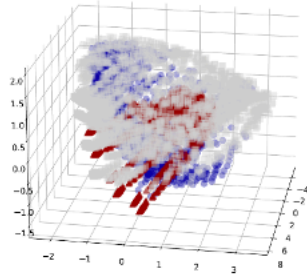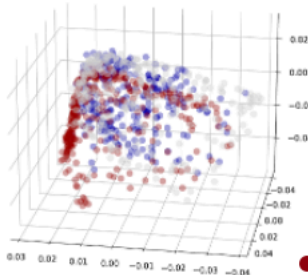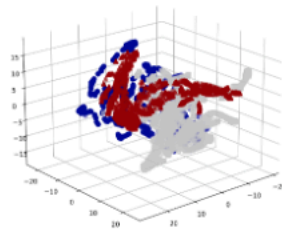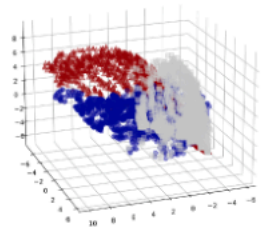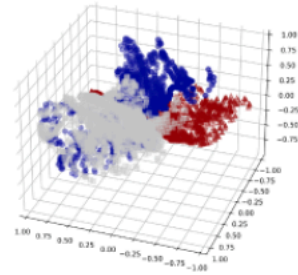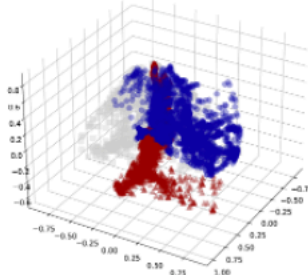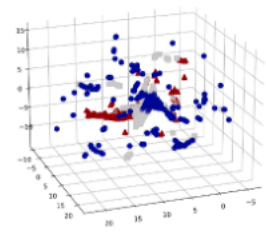
Figure 27 Representation of the 3-D manifold of the responses achieved by structure in Fig. 24a using different manifold learning approaches. Colors (blue/red/gray) represent the crystallization level of the GST (amorphous/crystalline/intermediate stage). (a) PCA, (b) kernel PCA, (c) LLE, (d) t-SNE, (e) MDS, (f) autoencoder, (g) convolutional autoencoder, and (h) UMAP.

5.2.2   Effect of Learning Loss and Metric in Knowledge Discovery

Besides methodology in manifold learning, selecting the loss function and the metric plays a crucial role in forming the manifold. As no one is aware of the intact underlying behaviors and basically that itself is the subject of study, having the luxury of forming the manifold from different perspectives could be a very good playground to solidify the light-matter interaction conjectures.

In Figures 28 I applied different loss functions to analyse the optical response that we get from the nanostructure in Fig. 24a for three different crystallization levels in both two and three dimensional space. As we can see different methods cluster responses in a different way, and this could help the designer analyse the underlying features from different aspects and come up with a stronger understanding/hypothesis about the relation of the material characteristics and the optical response. Here we could clearly see different crystallization levels cover different part of the manifold and by walking on the underlying manifold we can pave different regions that could be translated as having the desired response is just doable in a specific crystallization level.
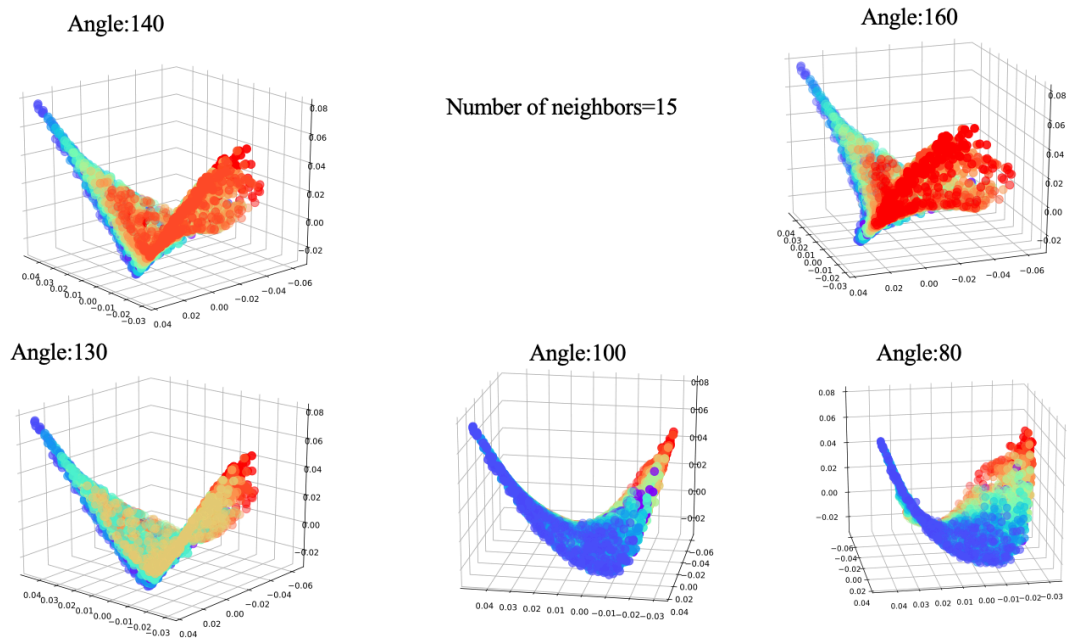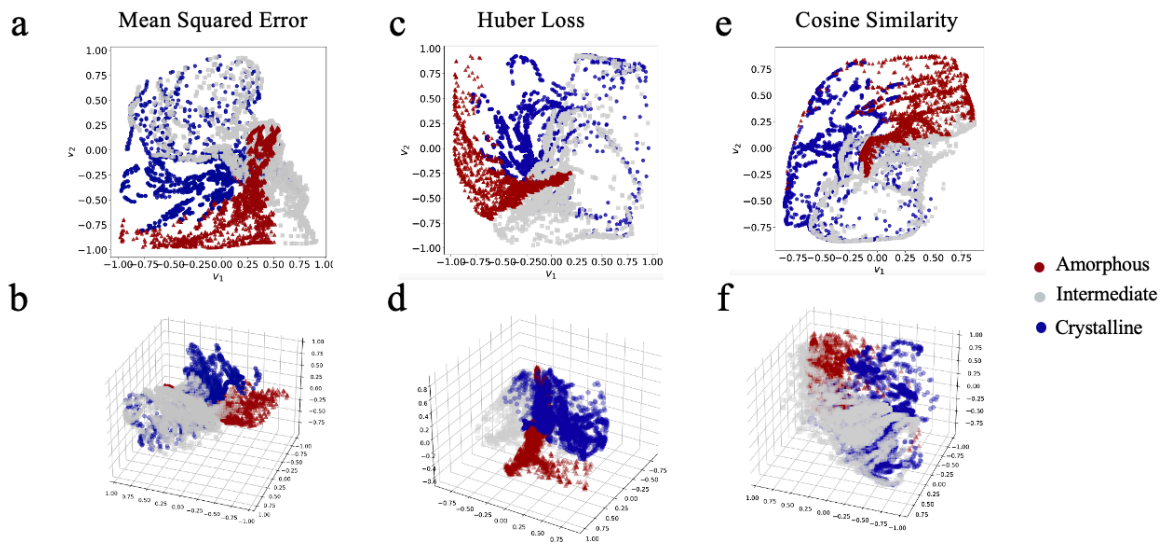
Figure 28 Representation of the 2D and 3D manifold of the responses achieved by structure in Fig. 24a using different losses. Colors (blue/red/gray) represent the crystallization level of the GST (amorphous/crystalline/intermediate stage). (a) 2-D MSE, (b) 3-D MSE, (c) 2-D Huber loss, (d) 3-D Huber loss, (e) 2-D Cosine similarity, (f) 3-D Cosine similarity.

5.3   Reducing the Geometric Complexity Using Manifold Learning

In this section, we present a manifold learning-based technique for inverse design of nanostructures with minimal design complexity. This technique encodes the high dimensional spectral responses obtained by EM simulation software for a class of nanostructure with different design complexities using an autoencoder. We model the governing distributions of the data in the latent space using Gaussian mixture model (GMM) [59] which then provides the level of feasibility of a desired response for each

structure and use a NN to find the optimum solution. This method also provides valuable information about the underlying physics of light-matter interactions by representing the sub-manifolds of feasible regions for each design complexity level (i.e., number of design parameters) in the latent space. To show the applicability of the method, we employ this technique for inverse design of a class of nanostructures consisting of dielectric metasurfaces with different complexity degrees.

The forward problem in designing nanophotonic structures is finding the response for a set of input design parameters. We consider this as the mapping $F : X \rightarrow Y$, where $\mathbf{x}$ $\in X$ is a vector of design parameters and $\mathbf{y} \in Y$ is the corresponding response. Electromagnetic simulation softwares like COMSOL Multiphysics, CST Microwave Studio, Lumerical, etc. are the common tools for solving the forward problem in the nanophotonics society. However, the goal of inverse problem is to find the set of design parameters that results in the desired response, and we consider this unknown relation as the mapping $G: Y \rightarrow X$. In other words, we seek to find $\mathbf{x}$ such that $\mathbf{x} = G(\mathbf{y}^*)$. Evaluating G is not possible as we don't have access to G. So, we formulate this problem in terms of F, which is available for us, within an optimization framework:

$$x^* = \mathop{argmin}_{x \in X} Loss(y, y^*) \tag{12}$$

where $\mathbf{y} = F(\mathbf{x})$, $\mathbf{y}^* = F(\mathbf{x}^*)$, and *Loss* can be any of the available loss functions that suit the problem (e.g. MSE). This problem does not have a closed-form formulation due to the complexity of the input to output relation in nanophotonic structures and also suffers from non-convexity and non-uniqueness challenges (i.e., for the desired response, there might be multiple sets of design parameters). The current methods for solving inverse problems

in nanophotonics are based on brute-force search methods for finding the vector $\mathbf{x}_i$ that results in the minimal MSE (i.e., $||\mathbf{y}_i - \mathbf{y}^*||_2^2$) or limits themselves to a particular part of the design space and model the inverse mapping to find the local minimum solution. However, these methods do not consider the design complexity of the structure in solving the inverse problem and converge to a highly complex system. In contrast, a coarser structure can produce comparable results. In this research, we use a manifold learning-based method to form the feasible set of responses for each design complexity in the latent space Z for a class of nanostructures and solve the inverse problem with the minimal design complexity. To show the capability of our method, we apply this approach to the inverse design of a class of nanostructure with different design complexities. Figure 28 shows the unit cell of the nanostructures, consisting of one to four ellipsoids of HfO_2 on the top of SiO_2 substrate [46]. As shown in Fig. 29, the number of design parameters and complexity of the structure increases as we add more ellipsoids. We randomly generate a set of design parameters for each structure and find the corresponding reflection responses using EM software (i.e., Lumerical). Then we train an AE to reduce the dimensionality of the response space Y. To model the distribution of the manifold of feasible responses for each structure, we use GMM. Finally, we train a NN from the design to the response space and use that to find the set of design parameters for the desired response.
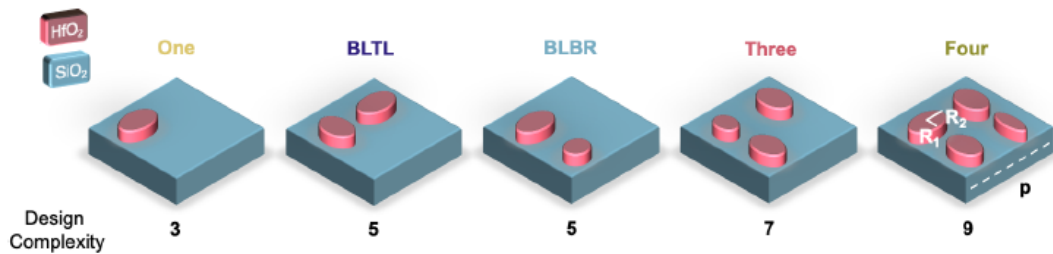
Figure 29 Schematic of the nanostructures [46] with different complexity levels (i.e., number of design parameters) composed of unit cells with a layer of SiO₂ and ellipsoid nano antennas of HfO₂. The design parameters are periodicity of the unit cells (p ∈ [500,900] nm) and radius of the ellipsoids (Ri ∈ [60,200] nm). The number of design parameters (i.e., design complexity) are shown below each structure.

To model the distribution of the manifold of the feasible response for each structure in Fig. 29, we use GMM. We consider the probability density function (pdf) of each structure as $f_Z(\mathbf{z}) = \sum_{i=1}^{N} \alpha_i g_i(\mathbf{z})$, where $\sum_{i=1}^{N} \alpha_i = 1$ and the g_i are Gaussian distributions with different means and covariance matrices ($g_i(\mathbf{z}) = N(\mathbf{z}; \mu_i, \Sigma_i)$). We used expectation maximization method to estimate the parameters $\theta = (\alpha_1,...,\alpha_N, \mu_1,...,\mu_N, \Sigma_1,...,\Sigma_N)$, given a series of observations $\mathbf{z}_1, \mathbf{z}_2,..., \mathbf{z}_M$. The goal in this optimization problem is to find a θ maximizing the log-likelihood $l(\theta; \mathbf{z}_1,..., \mathbf{z}_M) = P_{Mi=1} \log(P_{Nj=1} \alpha_j N(\mathbf{z}_i; \mu_j, \Sigma_j))$.

After reducing the dimensionality of the response space of the training data and modeling the manifold of the feasible set of responses for each structure in the latent space using GMMs, we use Algorithm 1 for evolutionary design of nanostructures. First, we reduce the dimensionality of the desired response using a trained autoencoder. Second, we find the log-likelihood of being inside the feasible set of each class of structures in Fig. 29. We select the structures with log-likelihood larger than a threshold as the candidates of the solution to our inverse problem. Finally, for each design candidate we use a trained NN to search over the design space for the solution (i.e., structure that has a similar reflection response to the desired response). We use MSE as our loss function to predict the responses for any given set of design parameters.

To train our model, we generate a random set of design parameters for structures in Fig. 28 and find their corresponding reflection spectra. We sample the period of the unitcells (p) between 500 nm and 900 nm and the radius of HfO_2 ellipsoids between 60 nm and 200 nm, with the fixed thickness of 350 nm in order to support reflection mode operation and satisfy the fabrication constraints. We excite the structures with normal incident light polarized in x-direction and conduct full-wave EM simulations with commercial Lumerical FDTD software to find the reflection responses of the structure in the wavelength of interest from 300 nm to 850 nm. These structures can potentially exhibit Fano-type resonances.

We trained an autoencoder to reduce the dimensionality of the response space from 550 to 2. Based on the manifold of the responses in Fig. 30, the *Four* scenario exhibits the most variate range of spectral responses in the latent space due to the dipole resonances in x-direction (co-polarized) and strong coupling of these resonances in y-direction (cross-polarized). It is also clear from Fig. 30 that *Three* scenario has a substantially smaller feasible region in comparison with the *Four* scenario due to reduction in the co-polarized resonance and cross-polarized coupling. The *BLBR* scenario resembles the *Three* scenario since the co-polarized resonance is much stronger than single ellipsoid along the co-polarized direction which results in a similar feasible range of responses as the *Three* scenario. This is also supported by the feasible region of *BLTL* which is much smaller than *BLBR* as the *BLTL* resonances are too weak to be coupled and reach the variety of *BLBR*. The *One* scenario exhibits the smallest convex hull with lowest resonance and coupling amongst all the scenarios as expected. In addition to the range of feasibility, the latent space representation provides insightful information about the classes of responses of in

different structures. As Fig. 30 shows, the resonances shift to left as we move counter-clockwise around the edge of the responses of the *Four* structure. Also moving from the outside of the feasible set toward the center results in significant reduction in the amplitude of the resonances. This shows that adding more ellipsoid nanoantennas results in expansion of the manifold of responses in a wide range of frequencies, and peaks with higher quality factors become achievable.

The results for two inverse designs are shown in Fig. 30a and b with the corresponding optimal design parameters, NMSE, and log-likelihood for each structure in structure results in a lower NMSE while *BLTL* and the *One* cannot produce a response similar to the desired spectra. For the desired response shown in Fig. 31b, however, the *Three* and *BLBR* structures result in a better design and lower NMSE in comparison to the *Four* which shows that the simpler structure would be a better option. This supports our claim regarding the ability of the evolutionary-based method for solving the inverse design with minimal design complexity. The response in Fig. 31b resembles a weaker cross-polarized coupling of dipole resonances compared to the desired response in Fig. 31a. This supports the lower NMSE of the predicted responses by *BLBR* and the *Three* for the desired response in Fig. 30b. However due to the lack of strong co-polarized and cross-polarized couplings in *BLTL* and the *One* scenarios, the selected desired responses are not feasible with these two structures.

Algorithm 1: Evolutionary Design Algorithm

Result: Optimum Design with Minimal Complexity

Step 1: Map the desired response into the latent space using the trained AE

Step 2: Find the log-likelihood of the feasibility of the response for each design complexity and select design candidates with higher log-likelihoods

Step 3: Use feed forward DNN to search over the design space of the candidates and find the optimal solution
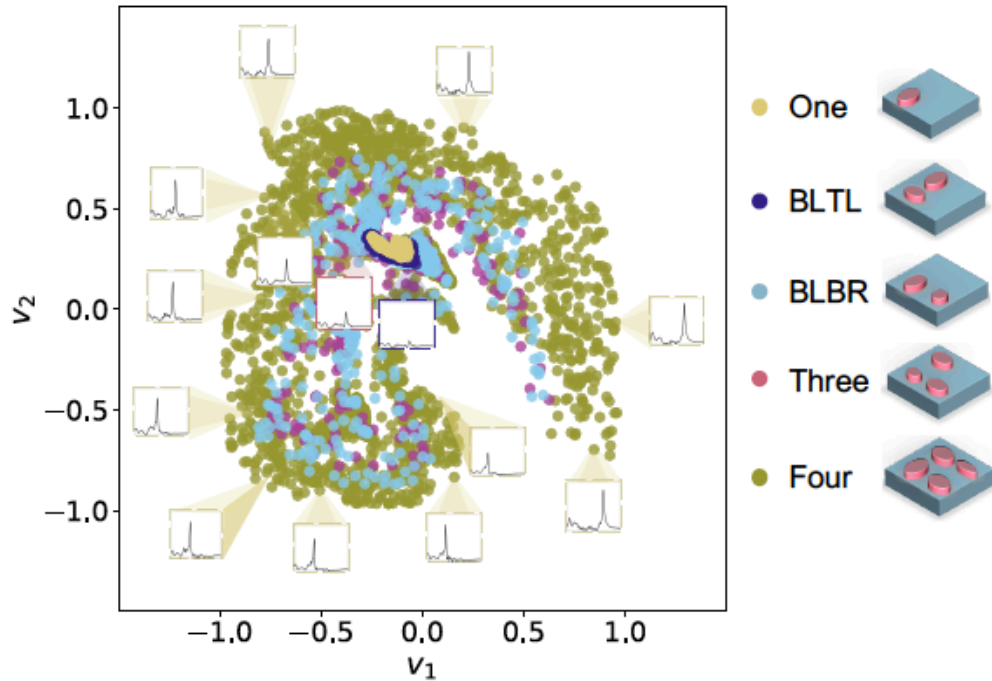
Figure 30 Representation of the responses in the latent space for the structures shown in Fig. 28. The Four structure, which has the highest complexity, has largest feasible region while the One has smallest feasible region. The changes in the responses corresponding to the movement in the latent space is shown as inset [46].

Table 5 Design parameters (in nm), NMSE, and log-likelihood for responses in Fig. 31a. T, B, L, and R refer to Top, Bottom, Left, and Right, respectively. R1 is the radius along x-axis and R2 is the radius along y-axis for each ellipsoid.

	ρ	R1BL	R2BL	R1BR	R2BR	R1TL	R2TL	R1TR	R2TR	NMSE	log(ρ)
One	897	179	64	0	0	0	0	0	0	0.892	-656
BLTL	546	79	79	0	0	153	132	0	0	0.876	-457
BLBR	809	153	143	163	121	0	0	0	0	0.459	-4.14
Three	780	168	144	168	144	145	98	0	0	0.397	-4.06
Four	833	823	160	823	160	823	160	160	121	0.238	-0.97

Table 6 Design parameters (in nm), NMSE, and log-likelihood for responses in Fig. 31b. T, B, L, and R refer to Top, Bottom, Left, and Right, respectively. R1 is the radius along x-axis and R2 is the radius along y-axis for each ellipsoid.

	ρ	R1BL	R2BL	R1BR	R2BR	R1TL	R2TL	R1TR	R2TR	NMSE	log(ρ)
One	683	64	0	0	0	0	0	0	0	0.892	-435

BLTL	882	787	111	0	0	174	89	0	0	0.88	-133
BLBR	737	132	121	132	132	0	0	0	0	0.378	-5.59
Three	700	168	121	168	98	121	98	0	0	0.411	-8
Four	700	823	823	823	160	121	121	160	121	0.416	-2.96
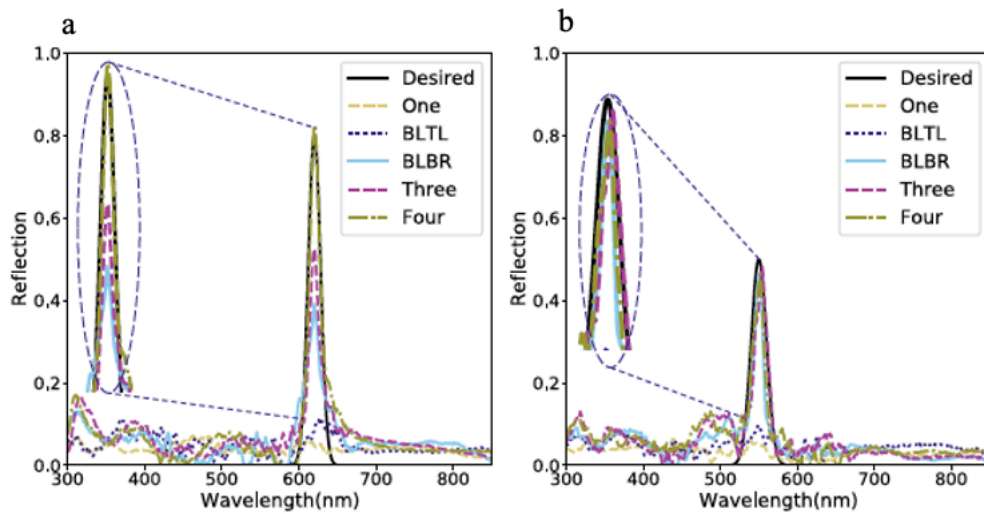
Figure 31 Results for two desired responses and optimized responses achieved by the structures in Fig. 29 using the evolutionary design algorithm. (a) A Gaussian shape reflection response with mean at 620 nm and sigma 6nm and (b) a Gaussian with mean at 550 nm and sigma 10 nm. The corresponding design parameters, NMSE, and log-likelihood are in Table 5 and Table 6, respectively.

5.4   Optical Sensitivity Analysis: Local Dimensionality Reduction for Studying the Role of Design Parameters in Response Variations

One of the critical features of designing nanostructure is being robust against errors and inconsistencies. Simulation software has been here for a long time, but there are still evident inconsistencies even when comparing the results of one software with another. It is clear that such results are not entirely accurate and, in the best case, a reasonable estimation of the optical responses for a particular nanostructure. This flaw, combined with the fabrication inconsistency, necessitates the urgency of having the techniques/solutions robust against the possible changes as no one is interested in having a delicate solution even if it has maximum accuracy.

5.4.1   Manifold Learning for Sensitivity Analysis

In this part we employed manifold learning technique to visualize the sweet spots for the designing nanostructures with a desired resonance wavelengths and quality factors (Q). First, we simulate 2000 random design patterns of the structure in Fig. 29. Then, we train a NN to model design-response relation for the structures. Figure 32 represent the corresponding 2-D patterns in the latent space. The bar represent different Q (high and low) and the resonance frequency (λ). We randomly tweak the design parameters and simulate the structure using the trained NN. Figure 33 shows that different part of the manifold (accordingly corresponding response regions) have different sensitivity for Q and λ. By having such information one could first select the desired operating wavelength and Q range and limit the algorithm to work in this region.
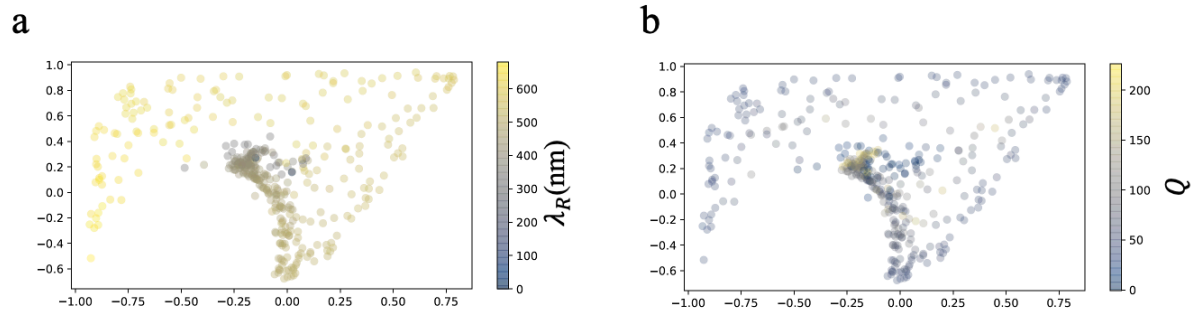
Figure 32 Low-dimensional representation of 400 random instances achieved by structure in Fig. 28. (a) Representation of the 2-D low-dimensional space colored for different resonance wavelengths. (b) Representation of the 2-D low-dimensional space colored for different resonance Q.
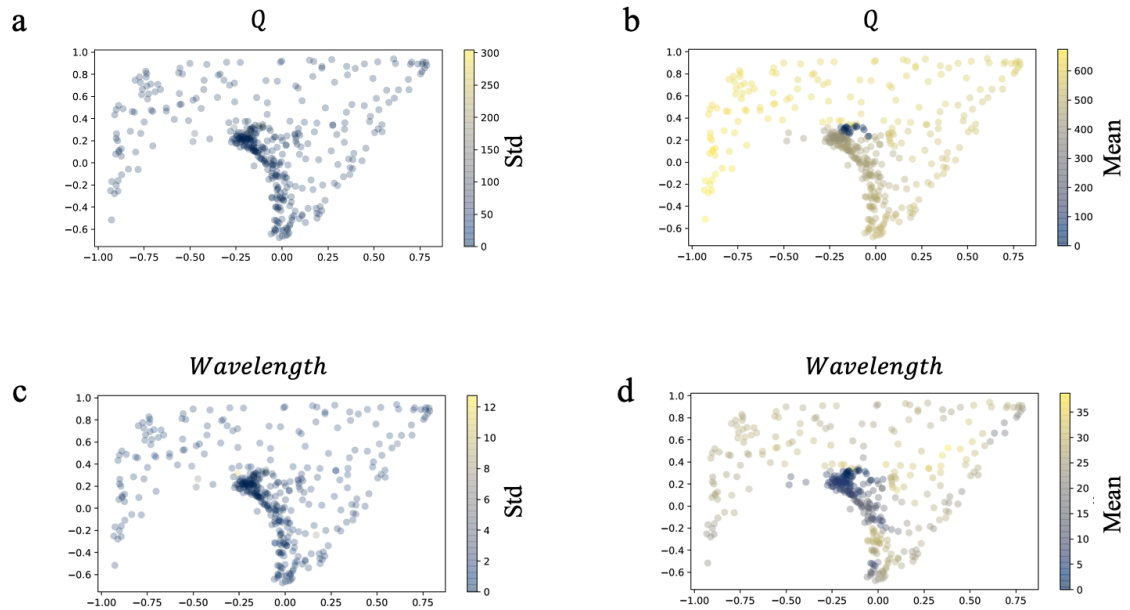
Figure 33 Sensitivity of the response in the low-dimensional space for 400 random designs achieved by structure in Fig. 29. (a) Representation of the Q in 2-D low-dimensional space colored for different standard deviation. (b) Representation of the

Q in 2-D low-dimensional space colored for different mean. (c) Representation of the resonance wavelength in 2-D space colored for different standard deviation. (d) Representation of the resonance wavelength in 2-D space colored for different mean.

5.4.2   Relating the Design Inconsistencies to the Latent Response Variations

The developed approach introduced in the previous section can be modified to enhance any desired feature in the DR algorithm, especially for understanding the roles of different design parameters. In this setting, the input to the DR autoencoder for the design space is *not* the design parameters; instead, it is the variation of design parameters to study the sensitivity to such variations. The algorithm (see Fig. 34) starts with selecting a desired feature in the input-output characteristics. For each point in the reduced response space, I find the *k* nearest neighbors in that space that have the smallest distance$|\delta_{i,j}|$ to the selected point *I*; $\delta_{i,j}$ is a quantitative measure defined based on the selected feature. In the next step, I find find the design space points that correspond to the point *i* and points *j = 1, 2, ..., and k* in the response space. We then calculate the vector of design parameter variations between points *i* and *j* in the design space (assuming *n* design parameters. This vector will have *n* components and is defined as $\Delta_{i,j}$). Each element of this vector is the difference between one of the design parameters' values at points *i* and *j*. Note that each point in the design space corresponds to a vector (of size *n*) that describes all design parameters corresponding to a single nanostructure design. To enhance the selected feature's role, we multiply this vector by its corresponding $|\delta_{i,j}|$. Then, I use the enhanced sensitivity vector components$|\delta_{i,j}| \Delta_{i,j}$ as the input to the DR autoencoder in the design space. Note that for each design point *i*, we will have *k* sets of input data (corresponding to the variation

between points i and $j = 1, 2, ..., k$) for training the autoencoder. The DR process here reduces the dimensions of the various vectors in the design space. Once the process is complete, the autoencoder's input points with higher weights correspond to design parameters with the most substantial influence on the selected feature. Considering the vast possibilities in choosing the number of nearest neighbors (k), the distance measure $\delta_{i,j}$, and the structure of the autoencoder, the ability of this approach in providing a deep understanding of the role of different design parameters on the input-output characteristics of the nanostructure is outstanding.
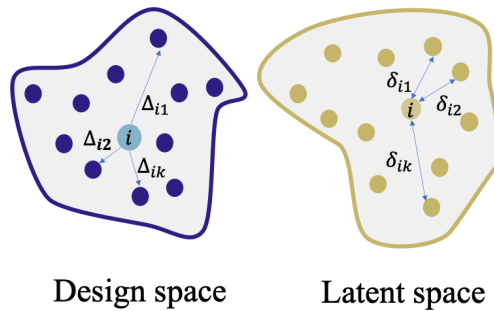
Figure 34 Representation of the latent design and response relation and relating the sensitivity of the design to the latent response.

5.5   Pruning Neural Networks for Understanding Design Response Relation

In the previous section we presented variety of techniques for learning the underlying physics of light-matter interactions. While these techniques are quite useful in discovering knowledge in nanophotonics, analyzing the intermediate connection of NNs become harder as we move toward the inner layers (deeper layers). Also, by analyzing the first layer we

will learn just a limited information about the role of design parameter. Here we employed pruning techniques for both removing nodes and connections to simplify the NN and study the effect of that simplification in the accuracy of the network. Figure 35 represents the pruning [60] technique for the node and synapse reduction scenarios.
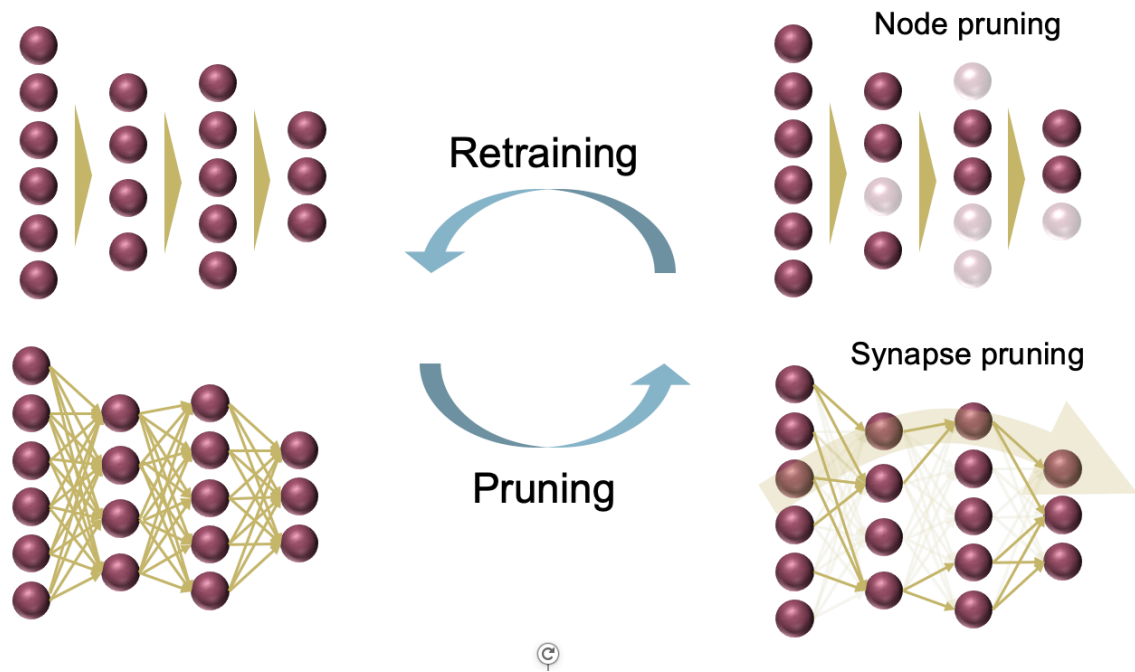
Figure 35 Schematic of the node and synapse pruning technique.

To show the effectiveness of the pruning technique in simplifying the NN while preserving the valid model for relating design to response, I applied the pruning algorithm to train a NN for modeling nanostructure response in Fig. 29. I trained two different NNs with different number of connections (deepness), on with 2.2M connections and one with 2.4K connections. The results in Fig. 33 represent the accuracy of these two networks for different pruning levels (sparsity levels). As it is shown in Fig. 36a and b we could preserve

the same accuracy for the model while removing more than 25% of the connections in both

scenarios.

a

Deep Neural Network with 2.2M Connections

b

Deep Neural Network with 2.4K Connections
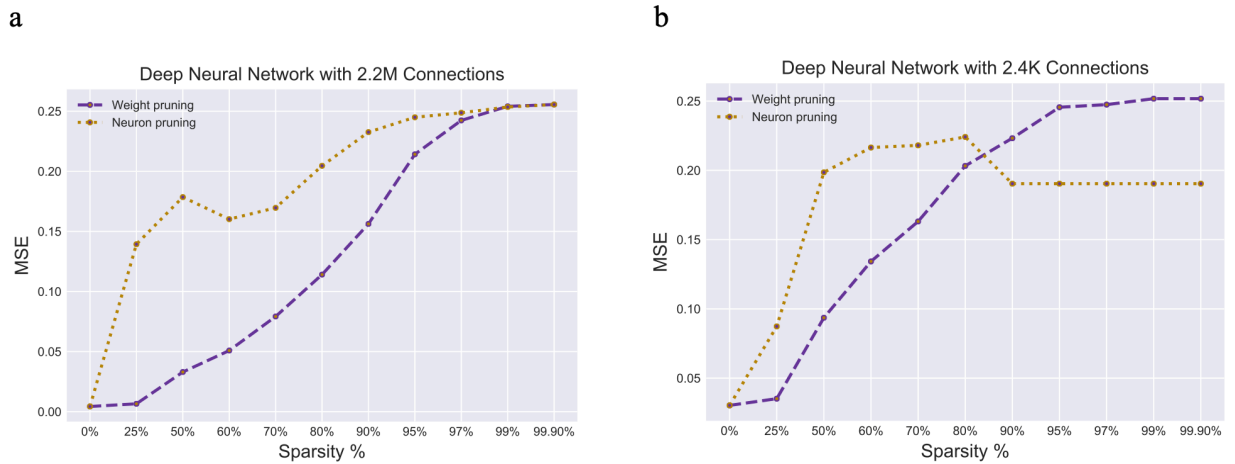
Figure 36 Results of pruning NNs trained to model the design to response relation of the structure in Fig. 29 for different pruning levels (i.e., sparsity levels) and different techniques (weight pruning and neuron pruning). (a) MSE of the pruned NN with 2.2 M connections trained to model design to response relation of the structure in Fig. 7. (b) MSE of the pruned NN with 2.4 k connections trained to model design to response relation of the structure in Fig. 29.

5.6   Conclusion

In conclusion, I demonstrated here an AI-based technique for the understanding of

the physics of wave-matter interaction in nanostructures [36-38]. Using the DR algorithm

in the response space and the design space (using an autoencoder and a pseudo-encoder, respectively), I could obtain an analytic formula that relates the design parameters to the response of the nanostructure while providing access to the weights of the NNs at all layers. By analysing these weights, meaningful information about the roles of different design parameters in the nanostructure's overall response can be obtained. This intuitive information can be used to understand the physics of light-matter interaction while facilitating the device optimization process by suggesting a non-uniform discretization of the design parameters to reduce the computation requirements. The approach presented here can significantly impact the design and understanding of the EM wave-matter interaction in nanostructures while being extendable to several other applications.

We showed that manifold learning [56-58] could significantly facilitate nanophotonic structures' inverse design and provide the optimal solution while evolving toward the least complex structure by providing multiple solutions (using feasibility score provided by GMM) with different degrees of freedom. By applying the technique to a dielectric metastructure design problem, we achieved the optimum nanostructure for a particular desired response while minimizing the geometrical complexity. Lastly, this can be extended to a wide range of design problems- fluid mechanics, material science, and electronics, to name a few.

CHAPTER 6.   EPILOGUE

6.1   Contribution to the Field

Design of photonic devices in the nanoscale regime outperforming the bulky optical components has been a long-lasting challenge in state-of-the-art applications. Accordingly, devising a comprehensive model to understand and explain the physics and dynamics of light-matter interaction in these nanostructures is a substantial step toward the realization of novel photonic devices. To this end, existing modeling methods can be categorized into two main groups: single- and multi-objective approaches. Single-objective approaches either rely on exhaustive design parameter sweeps using brute-force EM-solvers or evolve from an initial guess to a final result. Although the former requires extensive computation, the latter highly depends on the initial guess and, in most cases, converges to a local optimum. Parametrized adjoint optimization techniques can be used to design high-performance nanostructures; however, it is computationally expensive. All of these single objective approaches are computationally demanding and fail when the input-output relation is complex or the number of the desired features for a nanostructures grows. In contrast, multi-objective methods deal with the formation of a model to optimize a certain class of problems. Although these methods are more computationally efficient, obtaining an optimal solution is not guaranteed.

DL-based design approaches, combined with limited exhaustive searches, have proven to be a potent solver of multi-objective optimization problems by learning the input-output relation. DR approaches convert the inverse design problem into a more manageable version of it by effectively reducing the dimensionality of the problem. More importantly,

such novel techniques can provide considerable valuable insight about the dynamics of light-matter interaction in nanostructures with the hope of uncovering new phenomena that can be used to form a completely new types of devices. The change in focus of using DL techniques from "optimization" to "knowledge discovery" can open a new research area with potentially transformative results in the entire field of nanophotonics. Examples of these "knowledge discovery" paradigms include assessing the feasibility of a desired response using a given structure as well as the range of the possible responses a given design can provide. Knowing the feasibility of a desired response offered by a photonic nanostructure is very helpful prior to any design or optimization effort in avoiding suboptimal designs or convergence issues. It also guides us to modify the initial structure to achieve the desired response.

I have developed a new paradigm based on leveraging the "intelligent" aspects of AI to design nanostructure and understand the underlying physics of light-matter interactions. I showed, for the first time, that by reducing the dimensionality of the response and design spaces in nanophotonics using an autoencoder and a pseudo-encoder, we could convert the initial many-to-one problem into a one-to-one (or in the worst case, close to one-to-one) problem plus a considerably simpler one-to-many problem that can be solved using brute-force analytical formulas. The resulting approach considerably reduces the computational complexity of both the forward problem and the inverse (or design) problem. Besides, it allows for the inclusion of the design restrictions (e.g., fabrication limitations) without adding computational complexities. It also provides valuable information about the roles of design parameters in the EM structure response, which can potentially enable novel phenomena and devices. Finally, this technique can be extended to solve many different

optimization problems in a wide range of science and engineering disciplines as long as enough data for training the incorporated AI algorithms are provided.

I demonstrated an AI-based technique for the understanding of the physics of wave-matter interaction in photonic nanostructures. Using the DR algorithm in the response space and the design space (using an autoencoder and a pseudo-encoder, respectively), I obtained an analytic formula to relate the design parameters to the response of the nanostructure while providing access to the weights of the NNs at all layers. By analyzing these weights, meaningful information about the roles of different design parameters in the overall response of the nanostructure can be obtained. This intuitive information can be used to understand the physics of light-matter interaction while facilitating the device optimization process by suggesting a non-uniform discretization of the design parameters to reduce the computation requirements. The approach presented here can significantly impact the design and understanding of the light-matter interaction in photonic nanostructures while being extendable to several other applications.

I presented a new approach in utilizing AI for knowledge discovery in nanophotonics by training two well-known algorithms (convex-hull and one-class SVM). I showed that by combining the convex-hull (or the one-class SVM) with DR by an autoencoder, we could find the range of possible responses and the degree of the feasibility of any desired response from any given class of nanostructure in its latent RS. By applying these techniques to a series of nanostructures, I showed the unique capabilities of one-class SVM and convex-hull algorithms in providing valuable insight into the capabilities of any EM nanostructure in providing different types of responses. While this is the first demonstration of an AI-based approach for such knowledge discovery, the presented techniques show

great potentials in facilitating the understanding of the underlying physics of EM nanostructures as well as forming a more systematic approach in designing such nanostructures.

I presented a new approach to utilize manifold learning for knowledge discovery in nanophotonics by studying the low-dimensional manifold of optical spectra using the LLE algorithm. By applying this technique to a class of nanostructures, I showed the unique functionality of this method in supplying valuable insights about different features of the response of any EM nanostructure and its capabilities in providing different types of responses. The resulting approach can be used as a facilitator during the design and engineering of photonic nanostructures and understanding the roles of different design parameters in the response of the structure. It is worth mentioning that this method can analyze a wide range of optical design problems with different levels of complexity.

While my work provided the first examples of using AI for knowledge discovery in nanophotonic structures, the AI approaches I developed in this thesis are equally important in facilitating inverse design of photonic nanostructures, an urgent need of the industry. I showed that my DR techniques could reduce the computation requirements for the inverse design of photonic nanostructures by several orders of magnitude. Combined with the knowledge discovery techniques like one-class SVM and convex-hull, I showed the possibility of evolving from an initial architecture to a more optimal one (e.g., with reduced complexity, easier fabrication, etc.).

A key challenge that I addressed in the design of nanostructures was the non-uniqueness issue. I leverage MDNs to overcome the non-uniqueness challenge by

providing multiple designs for each desired optical response. I showed that by employing probabilistic methods (e.g., gaussian mixture models), a series of viable designs can be achieved for any desired response. Since material characteristics play a significant role in forming optical responses, I developed a fully automated tool based on my AI techniques for first selecting different materials in the envisioned platform and then finding the optimal geometrical design parameters for a complete solution of the inverse design problem.

I developed a fully probabilistic approach, which provided the degree of feasibility of any desired response from a type of nanostructure. Such a method can facilitate the design of nanostructures using conventional inverse-problem-solving approaches like genetic algorithms that focus on finding the design parameters of a selected structure without carefully studying the feasibility of achieving the desired response using the selected initial structure. My approach can also be combined with any other optimization approach as an initial feasibility-study step to ensure the initially selected structure for optimization is indeed a proper choice. More importantly, my method can reduce the initial selection complexity before running the optimization procedure to avoid unnecessarily complicated designs and reduce the fabrication challenges.

Extending the AI-based approaches to more sophisticated techniques, I demonstrated a reliable physics-driven manifold-learning approach to significantly facilitate the inverse design of nanophotonic structures and provide the optimal solution while evolving toward the least complex structure. The technique can offer multiple solutions (using MDNs) with different degrees of freedom. This model guides the user to select the best structure with the least design complexity (lowest fabrication complexity).

In summary, I have developed a rich portfolio of AI-based techniques for detailed knowledge discovery and inverse design of photonic nanostructures. I studied several important features in both obtaining valuable insight into the operation physics of these structures and in finding an optimal structure to provide a given response. I believe the combination of these approaches have opened a new area of research that can blossom in the coming years and change the way we analyze, design, and optimize nanophotonic structures. I am pleased that my techniques are being used by several research groups in the field to participate in this endeavor for a new era in intelligent knowledge discovery and design of electromagnetic nanostructures. I envision similar techniques can be adopted for a wide range of science and engineering disciplines. As such, I hope this thesis can facilitate innovative solutions for state-of-the-art problems in several applications.

6.2 Future Works

Despite the efforts on developing inverse design tools/algorithms, there is not any technique to solve ALL possible problems with arbitrary levels of complexity. All methods rely on intelligent trial and error on forward path, or they do the cyclic search over the design space. The main advantage of intelligent techniques is the computation efficiency and ability to reduce the complexity of the computation, e.g., by forming a complex analytic formula to replace the detailed EM solution. The reason of the limited success of several techniques (including some of the recent AI approaches) is simply the complexity of the design problem in which obtaining each instance (e.g., full simulation of a single structure) is time-consuming. This reduces the number of available samples that are obtained with a certain level of computation (e.g., using EM solvers). The AI-based techniques in this thesis were designed to increase the computation efficiency and thus,

expand the range of possible problems by enabling the design of ~~gematrically~~ more complex structures. Thus, there is still a major need to push for more computation efficiency and accepting some errors to obtain more sophisticated insight into the operation of the photonic nanostructures.

I envision three main paths for further improvement of the AI-based approaches for nanophotonics. First, we should develop approaches that can enable free-form structures (no pre-selected geometries) without requiring excessive computation due to the huge number of possible designs. This would be achieved by reducing the size of the design space while maximizing the spanned region in the response space. This could be done by creating some motif structures (rather than completely random binary patterns for a free-form structure) in the form of super cells and using them as building blocks to form any given nanostructure. In this formation, we do not consider changing one pixel of the free-form structure at a time. We rather consider combining different building blocks that have tangible impact on the response. Second, I believe we need to change our way of using same metrics for all the design problems. By using different metrics based on the importance of any given design parameter in the overall response (which can be found by the approaches I developed), the convergence of the algorithm with far fewer instances for training will be achieved. Finally, I believe efforts should be focused on reducing the number of connections between the design and response spaces to minimize the complexity of the input-output relation while providing maximum information about the physics of operation of the desired device. This will be a more rigorous extension of the pruning work that I did in this thesis. I believe these three efforts worth extensive investigations, which could form new PhD theses and hopefully, high-impact research projects.

REFERENCES

1. Taghinejad, Mohammad, and Wenshan Cai. "All-optical control of light in micro-and nanophotonics." ACS Photonics 6.5 (2019): 1082-1093.
2. Shen, Yichen, et al. "Deep learning with coherent nanophotonic circuits." Nature Photonics 11.7 (2017): 441-446.
3. Sreekanth, Kandammathe Valiyaveedu, et al. "Biosensing with the singular phase of an ultrathin metal-dielectric nanophotonic cavity." Nature communications 9.1 (2018): 1-8.
4. O'Carroll, Deirdre M. "Nanophotonics and plasmonics for solar energy harvesting and conversion." J. Photonics Energy 5.1 (2015): 057001.
5. Zhang, Shuyan, et al. "Metasurfaces for biomedical applications: imaging and sensing from a nanophotonics perspective." Nanophotonics 10.1 (2021): 259-293.
6. Lin, Dianmin, et al. "Dielectric gradient metasurface optical elements." science 345.6194 (2014): 298-302
7. Anthony, Martin, and Peter L. Bartlett. Neural network learning: Theoretical foundations. cambridge university press, 2009.
8. Huntington, Mark D., Lincoln J. Lauhon, and Teri W. Odom. "Subwavelength lattice optics by evolutionary design." Nano letters 14.12 (2014): 7195-7200.
9. Jin, Zhongwei, et al. "Complex inverse design of meta-optics by segmented hierarchical evolutionary algorithm." ACS nano 13.1 (2019): 821-829.
10. Cai, Haogang, et al. "Inverse design of metasurfaces with non-local interactions." npj Computational Materials 6.1 (2020): 1-8.
11. Tehrani, Kayvan F., et al. "Adaptive optics stochastic optical reconstruction microscopy (AO-STORM) using a genetic algorithm." Optics express 23.10 (2015): 13677-13692.
12. Macias, Demetrio, Dominique Barchiesi, and Alexandre Vial. "Evolutionary approach to an inverse problem in near-field optics microscopy." Optical Micro-and Nanometrology in Manufacturing Technology. Vol. 5458. International Society for Optics and Photonics, 2004.
13. Macias, Demetrio, Alexandre Vial, and Dominique Barchiesi. "Inverse scattering algorithm for near-field optics microscopy using intensity data." Progress in Electromagnetics Research Symposium. 2004.
14. Peurifoy, John, et al. "Nanophotonic particle simulation and inverse design using artificial neural networks." Science advances 4.6 (2018): eaar4206.
15. Liu, Dianjing, et al. "Training deep neural networks for the inverse design of nanophotonic structures." ACS Photonics 5.4 (2018): 1365-1369.
16. Tahersima, Mohammad H., et al. "Deep neural network inverse design of integrated photonic power splitters." Scientific reports 9.1 (2019): 1-9.
17. So, Sunae, and Junsuk Rho. "Designing nanophotonic structures using conditional deep convolutional generative adversarial networks." Nanophotonics 8.7 (2019): 1255-1261.
18. Lalau-Keraly, Christopher M., et al. "Adjoint shape optimization applied to electromagnetic design." Optics express 21.18 (2013): 21693-21701.

19. Chen, Yingshi, et al. "Smart inverse design of graphene-based photonic metamaterials by an adaptive artificial neural network." Nanoscale 11.19 (2019): 9749-9755.
20. Yao, Kan, Rohit Unni, and Yuebing Zheng. "Intelligent nanophotonics: merging photonics and artificial intelligence at the nanoscale." Nanophotonics 8.3 (2019).
21. Ma, Wei, Feng Cheng, and Yongmin Liu. "Deep-learning-enabled on-demand design of chiral metamaterials." ACS nano 12.6 (2018): 6326-6334.
22. Inampudi, Sandeep, and Hossein Mosallaei. "Neural network based design of metagratings." Applied Physics Letters 112.24 (2018): 241102.
23. Sakurai, Atsushi, et al. "Ultranarrow-band wavelength-selective thermal emission with aperiodic multilayered metamaterials designed by Bayesian optimization." ACS central science 5.2 (2019): 319-326.
24. Liu, Zhaocheng, et al. "Generative model for the inverse design of metasurfaces." Nano letters 18.10 (2018): 6570-6576.
25. So, Sunae, et al. "Deep learning enabled inverse design in nanophotonics." Nanophotonics 9.5 (2020): 1041-1057.
26. Jiang, Jiaqi, et al. "Free-form diffractive metagrating design based on generative adversarial networks." ACS nano 13.8 (2019): 8872-8878.
27. Jiang, Jiaqi, and Jonathan A. Fan. "Global optimization of dielectric metasurfaces using a physics-driven neural network." Nano letters 19.8 (2019): 5366-5372.
28. Nadell, Christian C., et al. "Deep learning for accelerated all-dielectric metasurface design." Optics express 27.20 (2019): 27523-27535.
29. Baxter, Joshua, et al. "Plasmonic colours predicted by deep learning." Scientific reports 9.1 (2019): 1-9.
30. Hegde, Ravi S. "Accelerating optics design optimizations with deep learning." Optical Engineering 58.6 (2019): 065103.
31. Kudyshev, Zhaxylyk A., et al. "Rapid classification of quantum sources enabled by machine learning." Advanced Quantum Technologies 3.10 (2020): 2000067.
32. Melati, Daniele, et al. "Mapping the global design space of integrated photonic components using machine learning pattern recognition." arXiv preprint arXiv:1811.01048 (2018).
33. Hammond, Alec M., and Ryan M. Camacho. "Designing integrated photonic devices using artificial neural networks." Optics express 27.21 (2019).
34. Lalau-Keraly, Christopher M., et al. "Adjoint shape optimization applied to electromagnetic design." Optics express 21.18 (2013): 21693-21701.
35. Aggarwal, Charu C. "On k-anonymity and the curse of dimensionality." VLDB. V.
36. Kiarashinejad, Yashar, Sajjad Abdollahramezani, and Ali Adibi. "Deep learning approach based on dimensionality reduction for designing electromagnetic nanostructures." npj Computational Materials 6.1 (2020): 1-12.
37. Kiarashinejad, Yashar, et al. "Mitigating inverse design complexity of nano-antennas using a novel dimensionality reduction approach (conference

presentation)." Photonic and Phononic Properties of Engineered Nanostructures IX. Vol. 10927. International Society for Optics and Photonics, 2019.

38. Kiarashinejad, Yashar, et al. "Deep learning reveals underlying physics of light–matter interactions in nanophotonic devices." Advanced Theory and Simulations 2.9 (2019): 1900088.

39. Hemmatyar, Omid, et al. "Full color generation with fano-type resonant HfO2 nanopillars designed by a deep-learning approach." Nanoscale 11.44 (2019): 21266-21274.

40. Zandehshahvar, Mohammadreza, et al. "Dimensionality reduction-based method for design and optimization of optical nanostructures using neural network." Frontiers in Optics. Optical Society of America, 2019.

41. Bishop, Christopher M. "Mixture density networks." (1994).

42. Hinton, Geoffrey E., and Ruslan R. Salakhutdinov. "Reducing the dimensionality of data with neural networks." science 313.5786 (2006): 504-507.

43. Roweis, Sam T., and Lawrence K. Saul. "Nonlinear dimensionality reduction by locally linear embedding." science 290.5500 (2000): 2323-2326.

44. Zandehshahvar, Mohammadreza, et al. "Inverse design of photonic nanostructures using dimensionality reduction: reducing the computational complexity." Optics Letters 46.11 (2021): 2634-2637.

45. Zandehshahvar, Mohammadreza, et al. "Sample-efficient machine-learning method for designing photonic nanostructures (Conference Presentation)." Photonic and Phononic Properties of Engineered Nanostructures X. Vol. 11289. International Society for Optics and Photonics, 2020.

46. Zandehshahvar, Mohammadreza, et al. "Accelerating inverse design of nanostructures using manifold learning." NeuRIPS machine learning for engineering and modeling, 2020.

47. Kiarashinejad, Yashar, et al. "Knowledge discovery in nanophotonics using geometric deep learning." Advanced Intelligent Systems 2.2 (2020): 1900132.

48. Kiarashinejad, Yashar, et al. "Geometric Deep Learning Unlocks the Underlying Physics of Nanostructures." CLEO: Science and Innovations. OSA, 2020.

49. Zandehshahvar, Mohammadreza, et al. "Cracking the Design Complexity of Nanostructures Using Geometric Deep Learning." CLEO: Science and Innovations. Optical Society of America, 2020.

50. Cotuk, Umit. Scattering from multi-layered metamaterials using wave matrices. Naval Postgraduate School Mnterey CA, 2005.

51. Barber, C. Bradford, David P. Dobkin, and Hannu Huhdanpaa. "The quickhull algorithm for convex hulls." ACM Transactions on Mathematical Software (TOMS) 22.4 (1996): 469-483.

52. Maaten, Laurens van der, and Geoffrey Hinton. "Visualizing data using t-SNE." Journal of machine learning research 9.Nov (2008): 2579-2605.

53. Balasubramanian, Mukund, et al. "The isomap algorithm and topological stability." Science 295.5552 (2002): 7-7.

54. McInnes, Leland, John Healy, and James Melville. "Umap: Uniform manifold approximation and projection for dimension reduction." arXiv preprint arXiv:1802.03426 (2018).
55. Chen, Yunqiang, Xiang Sean Zhou, and Thomas S. Huang. "One-class SVM for learning in image retrieval." Proceedings 2001 International Conference on Image Processing (Cat. No. 01CH37205). Vol. 1. IEEE, 2001.
56. Abdollahramezani, Sajjad, et al. "Dynamic hybrid metasurfaces." arXiv preprint arXiv:2008.03905 (2020).
57. Zandehshahvar, Mohammadreza, et al. "Manifold learning for knowledge discovery and intelligent inverse design of photonic nanostructures: breaking the geometric complexity." arXiv preprint arXiv:2102.04454 (2021).
58. Kiarashi, Yashar, Mohammadreza Zandehshahvar, and Ali Adibi. "Manifold learning for knowledge discovery and design in nanophotonics." Photonic and Phononic Properties of Engineered Nanostructures XI. Vol. 11694. International Society for Optics and Photonics, 2021.
59. Reynolds, Douglas A. "Gaussian mixture models." Encyclopedia of biometrics 741 (2009): 659-663.
60. Han, Song, Huizi Mao, and William J. Dally. "Deep compression: Compressing deep neural networks with pruning, trained quantization and huffman coding." arXiv preprint arXiv:1510.00149 (2015).
61. Wiecha, Peter R., Arnaud Arbouet, Christian Girard, and Otto L. Muskens. "Deep learning in nano-photonics: inverse design and beyond." *Photonics Research* 9, no. 5 (2021): B182-B200.
62. Dinsdale, Nicholas J., Peter R. Wiecha, Matthew Delaney, Jamie Reynolds, Martin Ebert, Ioannis Zeimpekis, David J. Thomson et al. "Deep learning enabled design of complex transmission matrices for universal optical components." ACS Photonics 8, no. 1 (2021): 283-295.